

57B, 114 (1968).

<sup>9</sup>The reader is referred to the original articles (Refs. 7 and 8) for more details.

<sup>10</sup>Throughout the paper, unless otherwise stated, we use the system of units where  $\hbar = m = c = 1$ . Then  $\alpha = e^2 = \frac{1}{137}$ . In this system energies, momenta, and cross sections are expressed in  $mc^2$ ,  $mc$ , and  $(r_0/\alpha)^2$  units, respectively, with  $mc^2 = 0.511$  MeV,  $mc = 0.511$  MeV/c, and  $(r_0/\alpha)^2 = 1490$  b.

<sup>11</sup>In the pair production case, an evaluation of the  $M_{2b,1b}$  term has been performed (Ref. 8). For  $k = 5.2$ , it is found that its contribution is 50 times smaller than the  $M_{2a,1c}$  and  $M_{2c,1a}$  contributions.

<sup>12</sup>A. Nordsieck, Phys. Rev. **93**, 785 (1954).

<sup>13</sup>(a) *Handbook of Mathematical Functions*, Natl. Bur. Std. Appl. Math. Series 55 (U.S. GPO, Washington, D. C., 1968), formula 15.1.1; (b) *ibid.*, formula 15.3.6.

<sup>14</sup>I. S. Gradshteyn and I. M. Ryzhik, *Table of Integrals, Series and Products* (Academic, New York, 1965), formula 8.325.1.

<sup>15</sup>This remark is valid at energies high enough, when  $n/E_1 < \pi/2$ .

<sup>16</sup>N. Starfelt and H. W. Koch, Phys. Rev. **102**, 1598 (1956).

<sup>17</sup>The Elwert-Haug formula gives the same values as  $d\sigma_1$ . Therefore, the corresponding curves are not plotted on the graphs.

## Polarization of Pb Vapor. III. Collisional Quenching and Depolarization of Alignment of Pb Metastable and Excited States

Hyatt M. Gibbs

*Bell Laboratories, Murray Hill, New Jersey 07974*

(Received 30 August 1971)

Several states of Pb were excited and studied in detail by simple optical techniques with data averaging. Cross sections for depolarization of alignment (in  $\text{\AA}^2$  at 850°K,  $\pm 20\%$ : He, 28; Ne, 46; Ar, 73; Xe, 105) and upper limits on quenching cross sections were determined for the  $^3P_1^o$  excited state of Pb<sup>208</sup> by monitoring the reduction in the polarization of the fluorescence as a function of foreign-gas pressure. Optical-pumping Zeeman resonances were detected in optically produced and polarized  $^3P_1$ ,  $^3P_2$ , and  $^1D_2$  metastable states and  $g_J$  ratios determined in Pb<sup>208</sup>:  $g_J(^3P_1)/g_J(^3P_2) = 1.17698(15)$  and  $g_J(^1D_2)/g_J(^3P_2) = 0.96158(33)$ . The  $g_J(^1D_2)$  due to Lurio and Landman implies  $g_J(^3P_2) = 1.2753(4)$  and  $g_J(^3P_1) = 1.5010(5)$ . From the dependence upon foreign-gas pressure of the optical-pumping recovery times after rf depolarization, the following cross sections for depolarization of alignment were deduced for the  $^3P_1$  and  $^3P_2$  states, respectively (in  $\text{\AA}^2$  at 813°K,  $\pm 20\%$ ): He, 27, 36; Ne, 27, 35; Ar, 51, 59; Kr, 64, 76; Xe, 123, 159; H<sub>2</sub>, 26, 39; N<sub>2</sub>, 73, 88. The  $^3P_1$  quenching cross sections were found to be less than  $10^{-21}$  cm<sup>2</sup> for the rare gases,  $\leq 1.3 \times 10^{-21}$  cm<sup>2</sup> for N<sub>2</sub>,  $24(5) \times 10^{-20}$  cm<sup>2</sup> for H<sub>2</sub>, and  $\leq 0.3 \times 10^{-20}$  cm<sup>2</sup> for D<sub>2</sub>. The  $^3P_1$  radiative lifetime of  $53 \pm 30$  msec was also extracted. Comparisons are made between some of the above experimental quantities and theoretical predictions.

### I. INTRODUCTION

Optical polarizations<sup>1</sup> of the  $^3P_1^o$  excited state<sup>2</sup> and  $^3P_1$  and  $^3P_2$  metastable states<sup>3</sup> were observed en route to optically pumping the  $^3P_0$  diamagnetic ground state as previously reported.<sup>1,4</sup> Collision phenomena are currently of importance in many fields including optical pumping, lasers, aeronomy, air pollution, plasmas, and reentry physics. Although Pb does not play an important role in most of these examples, cross-section measurements were made in the experimentally simple case of Pb in the hope that they will serve as useful tests of general theories. The usefulness of accurate  $g_J$  values in choosing wave functions motivated their measurement in Pb.

Collisional depolarization of alignment (hereafter called disalignment) and quenching of the  $^3P_1^o$  excited state are discussed in Sec. II; optical pump-

ing,  $g_J$  values, and collisional disalignment of the  $^3P_1$ ,  $^3P_2$ , and  $^1D_2$  metastable states in Sec. III; quenching of the  $^3P_1$  and  $^3P_2$  metastable states in Sec. IV; comparison of the experimental cross sections with theory in Sec. V; and concluding remarks in Sec. VI.

### II. DISALIGNMENT AND QUENCHING OF $^3P_1^o$ EXCITED STATE OF Pb<sup>208</sup>

Aligned  $^3P_1^o$  atoms are produced when  $^3P_0$  ground-state atoms absorb unpolarized 2833- $\text{\AA}$  resonance radiation (see Fig. 1). The alignment is monitored by detecting the polarization of the 3640- $\text{\AA}$  fluorescence.<sup>5</sup> A simple rate-equation derivation of the signal is given in Sec. IIA 1; the density matrix formalism is used in Sec. IIA 2. The apparatus is discussed in Sec. IIB and the cross-section results in Sec. IIC.

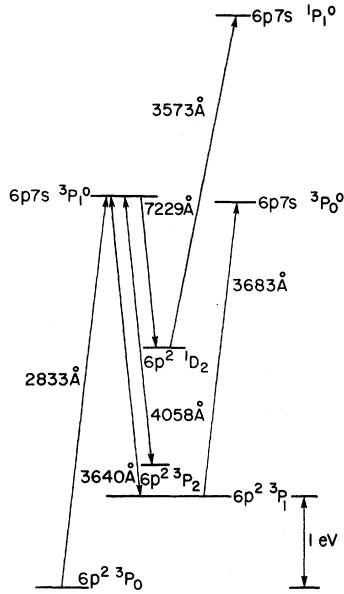


FIG. 1. Simplified energy-level diagram of Pb used in optical pumping.

#### A. Disalignment Signal

##### 1. Rate Equations

The relative transition probabilities for 2833-Å absorption and 3640-Å fluorescence are given in Fig. 2. Since only the  $M_J = \pm 1$  states are populated by the 2833-Å pumping light, the excited state is polarized. The polarization is, in fact, an alignment since  $M_J = \pm 1$  populations are equal. If no transitions to the  $M_J = 0$  state occur before re-emission, the fluorescence will be equally divided between  $\sigma(\Delta m = \pm 1)$  and  $\pi(\Delta m = 0)$  transitions. But if collisions equalize the populations in the excited-state sublevels, the  $\sigma$  transitions will be twice as intense as the  $\pi$  transitions. This change in the polarization of the fluorescence can be used to determine the disalignment cross section.

The perpendicular fluorescent intensity through a linear polarizer with its transmission axis parallel to the quantization axis is

$$F_{\perp} = C(N_+ + N_-), \quad (1)$$

where  $C$  is a proportionality constant and  $N_+$ ,  $N_0$ ,  $N_-$  are the populations of the  $M_J = +1, 0, -1$  substates of the  $^3P_1^0$  excited state, respectively. Similarly,

$$F_{\parallel} = \frac{1}{2} C(N_+ + N_- + 2N_0), \quad (2)$$

where  $F_{\parallel}$  is the intensity with the polarizer transmission axis perpendicular to the field. The factor of  $\frac{1}{2}$  in Eq. (2) arises because the angular factor for  $\sigma$  transitions is  $\frac{1}{2}$  that of  $\pi$  transitions for right-

angle observation.

An alignment may be defined as

$$A = (N_+ + N_- - 2N_0)/N, \quad (3)$$

with  $N = N_+ + N_- + N_0$ . In the density matrix notation of Ref. 5, one has  $A = \sqrt{2} \rho_z^0 / \rho_0^0$ . A convenient definition of a signal is

$$S \equiv \frac{F_{\parallel} + F_{\perp}}{F_{\parallel} - F_{\perp}} = \frac{1}{3} \left( 1 + \frac{8}{A} \right). \quad (4)$$

To determine  $A$  for a given density of rare-gas atoms  $n$ , consider the following rate equation:

$$\dot{N}_0 = -N_0/\tau - \sigma_Q n \bar{v} N_0 - \frac{2}{3} \sigma_A n \bar{v} N_0 + \frac{1}{3} \sigma_A n \bar{v} (N_+ + N_-), \quad (5)$$

where  $\tau$  is the  $^3P_1^0$  radiative lifetime,  $\sigma_Q$  is the quenching cross section,  $\bar{v}$  is the relative velocity between colliding atoms averaged over the Maxwellian distribution, and  $\sigma_A$  is the disalignment cross section. The equilibrium value of  $N_0$  (denoted  $\bar{N}_0$ ) is then found by setting  $\dot{N}_0 = 0$ :

$$\bar{N}_0 = \left( \frac{\frac{1}{3} \sigma_A n \bar{v}}{1/\tau + \frac{2}{3} \sigma_A n \bar{v} + \sigma_Q n \bar{v}} \right) (\bar{N}_+ + \bar{N}_-). \quad (6)$$

The signal is then

$$S = S(0) \left( 1 + \frac{8}{9} \frac{\sigma_A n \bar{v}}{1/\tau + \sigma_Q n \bar{v}} \right), \quad (7)$$

where  $S(0)$  is the signal for  $n=0$ . For  $\sigma_Q \approx 0$  ( $\sigma_Q n \bar{v} \ll 1/\tau$ ),  $\sigma_A$  is obtained as the slope of a plot of  $S$  vs  $n$  assuming  $\tau$  is known and  $\bar{v}$  is calculated from kinetic theory. If  $\sigma_Q n \bar{v} \gg 1/\tau$ , then  $S \rightarrow S(0) \times (1 + \frac{8}{9} \sigma_A / \sigma_Q)$  for large  $n$ ; i.e., the signal approaches a constant at high densities. In this limit complete disalignment is impossible because quenching occurs first.

It will be shown in Sec. II A 2 that this rate-equation derivation with its simple physical interpretation is valid if radiation trapping is negligible.

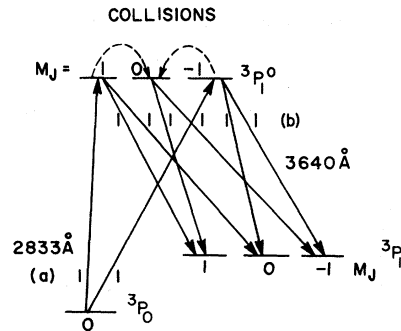


FIG. 2. Relative probabilities (at a given wavelength) for the (a) pumping and (b) fluorescence transitions involved in the production and detection of alignment in the  $^3P_1^0$  state.

## 2. Density Matrix

Happer and Saloman<sup>6</sup> have shown that the intensity of the fluorescent light is

$$I_b(\Omega)d\Omega = d\Omega z(1-x_b) \frac{9}{8\pi} \sum_L \frac{\Gamma_b}{\Gamma^{(L)}} W_L y_L. \quad (8)$$

The excitation rate  $z$  from ground state  $g$  (with angular momentum  $J_g$ ) to excited state  $e$  is equal to the total number of photons emitted into all the cross-fluorescent modes  $b$ :

$$z = \sum_{b,\lambda} \int I_b(\Omega) d\Omega. \quad (9)$$

$(1-x_b)$  is the probability that a fluorescent photon will escape from the vapor without being reabsorbed. The cross-fluorescent branching ratio is  $\Gamma_b/\Gamma$ , where  $1/\Gamma$  is the natural radiative lifetime of the excited state.  $\Gamma^{(L)}$ , the decay rate of the  $L$ th multipole moment of the excited state, is given by

$$\Gamma^{(L)} = \Gamma - \sum_b x_b \alpha_b^{(L)} \Gamma_b + Z_L. \quad (10)$$

These terms describe radiative decay, radiation trapping, and collision broadening, respectively. The values of the angular depolarization factor  $\alpha_b^{(L)}$  are given in Ref. 6. The  $W_L$  are products of Racah coefficients and are given in Ref. 6 for the present case. The dependence of the intensity upon the polarization vectors of the light is contained in  $y_L$ :

$$y_L = \sum_M \frac{(-1)^M E_{-M}^L U_M^L}{1 + iM\omega/\Gamma^{(L)}}, \quad (11)$$

$$E_M^L = \sum_{\mu} e_{\mu} (e_{\mu-M})^* (-1)^{\mu-M-1} C(11L; \mu, M-\mu), \quad (12)$$

$$U_M^L = \sum_{\mu} \mu_{\mu} (\mu_{\mu-M})^* (-1)^{\mu-M-1} C(11L; \mu, M-\mu), \quad (13)$$

where  $\hat{e}$  is the polarization vector of the exciting light and  $\hat{u}$  is the polarization vector of the detected fluorescence. Their derivation assumes that the ground state is unpolarized which is certainly the case for the  $^3P_0$  ground state of  $\text{Pb}^{208}$  ( $I=0$ ).

This formalism will now be applied to obtain an expression for the signal defined by Eq. (4). For excitation by unpolarized radiation along the field  $e_{\pm 1} = e^{\pm i\alpha}/\sqrt{2}$  with  $\alpha$  random; then  $E_0^0 = 1/\sqrt{3}$  and  $E_0^2 = 1/\sqrt{6}$  are the only nonvanishing components. For observation at right angles to the field through a polarizer aligned along the field  $u_0 = 1$ , giving  $U_0^0 = 1/\sqrt{3}$  and  $U_0^2 = -\sqrt{2}/\sqrt{3}$ , whereas for the polarizer perpendicular to the field  $u_{\pm 1} = 1/\sqrt{2}$  so  $U_0^0 = 1/\sqrt{3}$  and  $U_0^2 = 1/\sqrt{6}$ . From Table I of Ref. 6,  $W_0 = \frac{1}{3}$  and  $W_2 = -\frac{1}{6}$  for  $J_g = 0$  and  $J_b = 1$ . Therefore,

$$S \equiv \frac{F_{\parallel} + F_{\perp}}{F_{\parallel} - F_{\perp}} = \frac{1}{3} + \frac{8\Gamma^{(2)}}{3\Gamma^{(0)}}. \quad (14)$$

From Ref. 6,  $\alpha^{(0)} = 1$ ,  $\alpha^{(2)}(J_e = J' = 1, J_b = J = 0) = \frac{7}{10}$ , where it is assumed that only the 2833-Å photons

are trapped.  $Z_0 = Z_Q$  and  $Z_2 = Z_Q + Z_A''$ , where  $Z_0$  is the quenching rate and  $Z_A''$  is the collisional disalignment rate. Then we find

$$\Gamma^{(0)} = \Gamma(1 - xR) + Z_Q, \quad (15)$$

$$\Gamma^{(2)} = \Gamma(1 - \frac{7}{10}xR) + Z_Q + Z_A'', \quad (16)$$

where  $R$  is the branching ratio from the  $^3P_1^o$  to the  $^3P_1$  state, and  $x$  is the trapping probability for 2833-Å photons. Therefore, we find

$$S = S(0) \left[ 1 + \frac{8}{9} \left( \frac{\frac{7}{10}xR\Gamma + Z_A''}{\Gamma(1 - xR) + Z_Q} \right) \right]; \quad (17)$$

$S(0)$ , the signal in the limit of low Pb density, is theoretically 3.  $\Gamma$  is the reciprocal lifetime  $T_R$  of the  $^3P_1^o$  state;  $T_R = 5.7$  nsec.<sup>7</sup> The rates  $Z$  are related to corresponding cross sections  $\sigma$  by

$$Z = \sigma n \bar{v}, \quad (18)$$

where  $n$  is the density of the perturber ( $\text{Pb}^3P_0$  ground-state atoms for resonant collisions or foreign-gas atoms for nonresonant collisions) and

$$\bar{v} = v_{av} = \left( \frac{8kT(1/M + 1/M')}{\pi} \right)^{1/2}$$

is the average relative velocity between perturber of mass  $M'$  and Pb excited-state atom of mass  $M$ . In most of the present work the Pb density<sup>8</sup> was below  $10^{11}$  atoms/cm<sup>3</sup> so that  $xR \approx 0$ ; then

$$S \approx S(0) \left( 1 + \frac{\frac{8}{9}Z_A''}{\Gamma + Z_Q} \right) = S(0) \left( 1 + \frac{\frac{8}{9}\sigma_A n \bar{v}}{1/\tau + \sigma_Q n \bar{v}} \right) \quad (19)$$

in agreement with Eq. (7).

## B. Apparatus

A schematic diagram of the experimental apparatus is presented in Fig. 3. The electrodeless natural-Pb lamp<sup>9</sup> was excited by 2450-MHz microwaves from a Raytheon PGM-10. A Princeton Applied Research BZ-1 chopper and HR-8 lock-in amplifier were used to improve the signal-to-noise ratio. A 125-Å bandwidth interference filter and

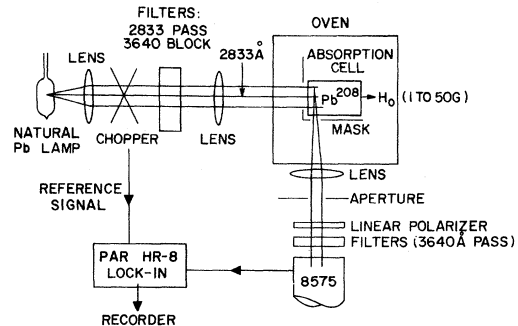


FIG. 3. Schematic diagram of experimental apparatus for measuring Pb disalignment cross sections in the  $^3P_1^o$  excited state.

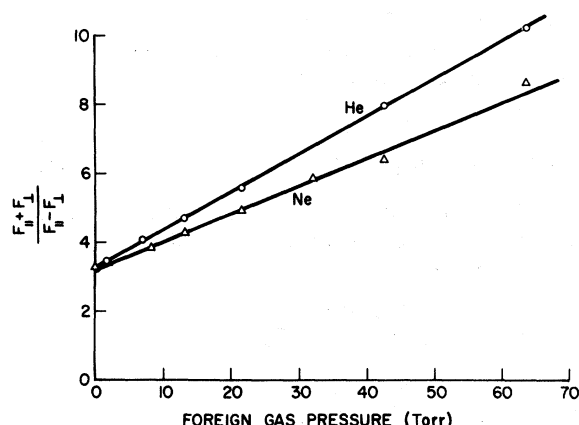


FIG. 4. Representative disalignment signals in the  $^3P_1^0$  excited state.  $F_{\parallel}$  and  $F_{\perp}$  are the intensities of the 3640-Å fluorescence as detected through a linear polarizer parallel and perpendicular to the pumping beam direction (collinear with magnetic field).

$\text{NiSO}_4$  liquid absorption cell passed the 2833-Å pumping line while eliminating the strong lines at 3640, 3683, and 4058 Å. Interference filters in the detection arm isolated the 3640-Å fluorescence which was detected by an RCA 8575 photomultiplier tube.

The 99.5% pure  $\text{Pb}^{208}$  metal was contained in the sidearm of a cylindrical Suprasil quartz cell 1.8 cm diam and 2.5 cm long. The cell was attached to the vacuum system through a 5-cm-long and 1-mm-diam capillary. A ground-quartz plug at the top of the capillary lengthened the escape time of the Pb separated isotope; the plug was raised periodically by its Kovar slug to permit impurities to escape.<sup>10</sup> This procedure eliminated the common problem of gassy sealed-off cells and permitted studies up to 900 °C with no difficulty. The cell was heated by a bulky oven 25 cm diam and 34 cm long with a water-cooled copper shell, Corning's Cercor insulation, and custom-built Lindberg Hevi-Duty heaters surrounding a 10-cm cubical shell of nickel which reduced thermal gradients. A separate heater controlled the temperature of

TABLE I. Disalignment and quenching cross sections (20% uncertainties unless shown otherwise) for the  $(6p7s)$   $^3P_1^0$  state of  $\text{Pb}^{208}$  at 850 °K.

	$\sigma_D(\text{\AA}^2)$	$\sigma_Q(\text{\AA}^2)$
He	28	< 0.3
Ne	46	< 1
Ar	73	< 1
Xe	105	< 4
H <sub>2</sub>	27	< 0.3
D <sub>2</sub>	38	< 0.9
N <sub>2</sub>	60(30)	16(8)

the  $\text{Pb}^{208}$  in the sidearm. A mask around the cell eliminated much of the reflected and multiply scattered light and confined the observation to fluorescence from the front 2 or 3 mm of the cell. Apertures in the excitation and detection beams limited the divergent angles to a few degrees.

Pressures were measured with a mercury manometer or a CVC GHD-100 gauge calibrated with the manometer.

### C. Results

#### 1. Disalignment Cross Sections

In the limit of no trapping ( $\alpha R = 0$ ) the theoretical expression for the signal defined by Eq. (4) is given by Eq. (19). The foreign-gas-disalignment cross-section measurements were made with the sidearm temperature between 460 and 480 °C for which the density is less than  $10^{11}$  atoms/cm<sup>3</sup>. Both calculation<sup>11</sup> and experimentation indicate that the trapping is then negligible for the present geometry.

The fluorescent intensities needed to calculate the signal as defined in Eq. (4) were obtained by alternately observing the fluorescence through a linear polarizer with transmission axis parallel to the field and through one perpendicular to the field. The equality of the transmissions of the two linear polarizers was checked. The photomultiplier output for zero fluorescence was determined by blocking the excitation beam. Representative data for He and Ne are shown in Fig. 4. Equation (4) can be used to convert an observed signal into an alignment as shown in Fig. 5. The plots of signal vs foreign-gas pressure for He, Ne, Ar, Xe, H<sub>2</sub>, and D<sub>2</sub> were straight lines permitting the calculation of the disalignment cross sections  $\sigma_A$  listed in Table I ( $T_R$  is known,  $\bar{v}$  is calculated from kinetic theory, and  $n = P/kT_0$  where  $P$  is the gauge pressure

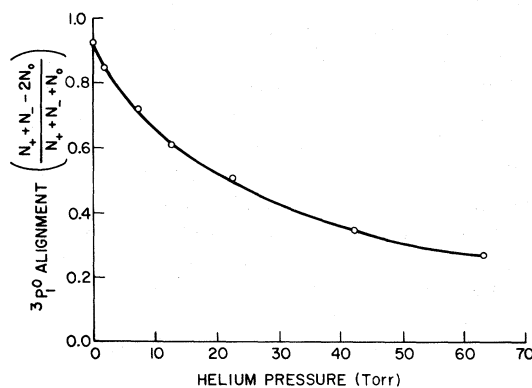


FIG. 5. Alignment of the  $^3P_1^0$  state as a function of helium pressure [calculated from Fig. 4 and Eq. (4)]. The efficacy of the polarizers and the unimportance of wall scattering are shown by the large alignment at zero foreign-gas pressure.

and  $T_0$  is the oven temperature).

## 2. Quenching

Upper limits can be placed on the quenching cross sections using Eq. (7) and noting that the experimental signal curves ( $S$  vs  $n$  or  $P$ ) deviate from a straight line by less than 10%; the upper limits are listed in Table I.

In the case of  $N_2$ , quenching of the  $^3P_1^0$  state is not negligible compared with disalignment. The signal approached a constant with increased  $N_2$  pressure as shown in Fig. 6(a). If  $S(0)/[S - S(0)]$  is plotted as a function of  $1/n$  or  $1/P$  the intercept is  $9\sigma_Q/8\sigma_A$  and the slope  $9/8\tau\sigma_A\bar{v}n^5$ ; see Fig. 6(b). The cross sections for quenching and disalignment of the  $Pb^{208}$   $^3P_1^0$  excited state by  $N_2$  are also presented in Table I.

The analysis here assumes that if an atom in the  $^3P_1^0$  excited state is quenched it returns to the  $^3P_1^0$  state only by optical-excitation and not collisional-excitation transfer. It is possible that an atom could have its excitation energy transferred to the  $^3P_0^0$  state and back again. Such a process (which could be studied by monitoring 3683-Å fluorescence from the  $^3P_0^0$  state) would complicate the analysis; the cross section deduced above would then be too small. The  $^3P_1^0$  quenching cross section of  $16 \text{ Å}^2$  at  $850^\circ \text{K}$  is to be compared with  $5.7 \pm 0.5 \text{ Å}^2$  found by Jenkins in a  $1400^\circ \text{K}$  flame.<sup>12</sup>

## 3. Radiation Trapping and Resonant Broadening at High Pb Densities

The equivalence of this depolarization of fluorescence technique for determining disalignment and quenching cross sections to the Hanle method has been demonstrated previously.<sup>5</sup> The linewidths measured in a Hanle experiment correspond to the  $\Gamma$ 's in the static fluorescence polarization method. The latter technique has the advantage of requiring no variation of a large magnetic field, but the Hanle method is simpler for studying disorientation.

At high Pb densities, the Hanle method has the distinct advantage that it is less dependent upon solid-angle effects, as can be seen as follows. At high Pb densities the  $^3P_1^0$  density decreases away from the entrance window as the pumping radiation is depleted. The excited-state alignment decreases even more rapidly through the cell because a larger portion of the excitation is by absorption of scattered rather than pumping radiation. But in the Hanle technique the intensity given by Eq. (8) is monitored as a function of magnetic field. In an alignment experiment  $\hat{e}$  and  $\hat{u}$  are chosen so that only  $L = 0$  and  $L = 2$  terms enter in Eq. (8). The  $L = 0$  and  $L = 2$ ,  $M = 0$  terms are field independent. The  $L = 2$ ,  $M = \pm 1$  terms enter equally by symmetry; a reduction in the initial alignment merely reduces the magnitude of the Hanle signal to first order. In

contrast the fluorescence technique depends upon the ratio of intensities. A change in the initial proportions of  $L = 0$  and  $L = 2$  terms in the initial state also changes the ratio. The Hanle signal is proportional to  $C_1\bar{\rho}_0^0 + C_2\bar{\rho}_2^0 + C_3(\bar{\rho}_2^{-2} + \bar{\rho}_2^2)$ , where  $\bar{\rho}_L^M$  are the irreducible tensor components<sup>5</sup> of the equilibrium density matrix and are proportional to the initial values of  $\rho_L^M$ ; since only the  $\bar{\rho}_2^{-2} + \bar{\rho}_2^2$  term depends upon the field, a reduction in  $C_3$  at high densities just reduces the signal strengths. The fluorescence signal is  $\frac{1}{3}(1 + 4\sqrt{2}\bar{\rho}_0^0/\bar{\rho}_2^0)$ ; as the Pb density is increased, the initial ratio of excited-state population ( $\propto \rho_0^0$ ) to alignment ( $\propto \rho_2^0$ ) is not constant as assumed in deriving Eq. (17) but increases as a result of the depolarization of the exciting radiation. This effect was observed by noting the reduction in  $S$  from 5.2 to 4.5 at constant Pb density as the solid angle was reduced. The extrapolated value for zero solid angle was not found, but from the values  $R = 0.27$  and  $\sigma v = 3.8 \times 10^{-8} \text{ cm}^3/\text{sec}$  from Happer and Saloman<sup>6</sup> and with  $x = 1$  and  $6.4 \times 10^{14} \text{ atoms/cm}^3$ ,  $S$  should have been 4.1.<sup>11,13</sup>

The solid-angle corrections discussed above are negligible for low Pb density; the branching ratio  $R$  can then be determined with the aid of a foreign

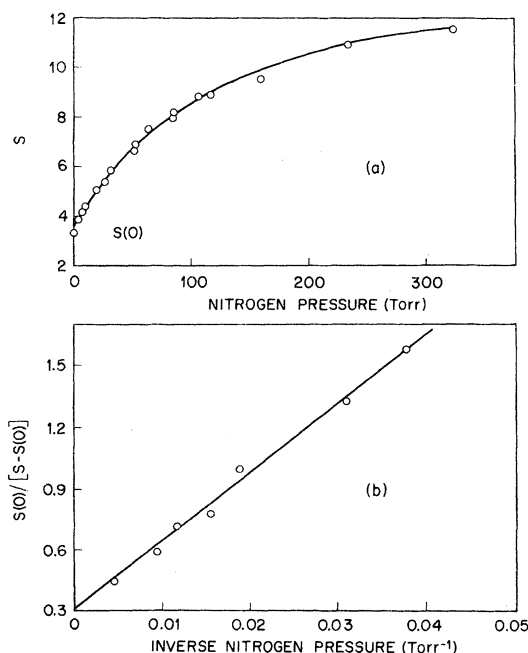


FIG. 6. (a) Fluorescence signal  $S = (F_{||} + F_{\perp}) / (F_{||} - F_{\perp})$  vs nitrogen pressure showing the approach to a constant value at high pressures when quenching is not negligible. (b) Some of the data of (a) is replotted as a straight line with slope proportional to the inverse disalignment cross section and the intercept to the ratio of quenching to disalignment cross sections.

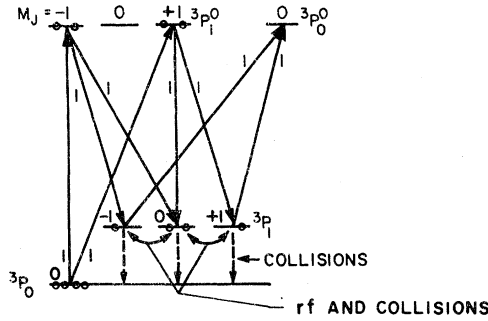


FIG. 7. Detection of  $^3P_1$  optical pumping using unpolarized light. Numbers beside arrows indicate relative strengths of transitions at a given wavelength.

gas. Equation (17) is, for  $Z_Q = 0$  and  $\chi R \approx 0$  (low Pb density),

$$S \approx S(0)(1 + 8n\sigma_A\bar{v}/9\Gamma), \quad (20)$$

whereas for  $Z_Q = 0$  and  $\chi R \approx 1$  (complete 2833-Å trapping at high Pb density),

$$S' \approx S(0) \left[ 1 + \frac{4}{15} \left( \frac{R}{1-R} \right) + \frac{8p\sigma_R\bar{v}}{9\Gamma(1-R)} + \frac{8n\sigma_A\bar{v}}{9\Gamma(1-R)} \right], \quad (21)$$

where  $p$  is the Pb ground-state density and  $\sigma_R$  and  $\sigma_A$  are the resonant-broadening and foreign-gas-disalignment cross sections, respectively. Then if 1 and 2 represent two different foreign-gas pressures we see that

$$(S'_2 - S'_1)/(S_2 - S_1) = 1/(1-R). \quad (22)$$

This change in slope is a result of the increased depolarization possible when the excited-state lifetime is lengthened by radiation trapping. It was easily seen experimentally and was consistent with  $R \approx 0.3$  although insufficient precautions were taken to avoid solid-angle errors and yield a precise measurement of  $R$ .

### III. OPTICAL PUMPING AND COLLISIONAL DISALIGNMENT OF Pb METASTABLE STATES

In Sec. II the alignment of the  $^3P_1^o$  excited state was studied. Some of the  $^3P_1^o$  atoms undergo spontaneous transitions to the  $^3P_2$ ,  $^3P_1$ , and  $^1D_2$  states that belong to the ground-state configuration and, therefore, are metastable states. The resultant polarization in the metastable states can be monitored by absorption of 4058-, 3640- or 3683-, and 3573-Å resonance radiation, respectively, (see Fig. 1). Optical studies of these metastables are described in Sec. III A and the apparatus in Sec. III B. Precision measurements of the  $g_J$  values are described in Sec. III C. The determination of  $^3P_1$  and  $^3P_2$  disalignment cross sections is discussed in Sec. III D. Disalignment by wall collisions is discussed in Sec. III E.

#### A. Optical Production and Polarization of Metastable States

Optical polarization of the Pb metastable states was reported previously<sup>3</sup>; other  $L = 1$  states have been optically pumped and are listed in Ref. 4 of Paper I.

The simplest case for illustrative purposes is the  $\text{Pb}^{208}$  ( $I = 0$ )  $^3P_1$  metastable state. The relevant energy levels and electric dipole transition probabilities appear in Fig. 7. Suppose we consider four  $^3P_0$  ground-state atoms (depicted by the circles in Fig. 7) irradiated by unpolarized 2833-Å resonance radiation incident along a weak external magnetic field. On the average two of the atoms will reach each of the  $M_J = \pm 1$  substates of the  $^3P_1^o$  excited state. Spontaneous emission from these substates (disregarding branching) results in one atom in each of the  $M_J = \pm 1$  substates of the  $^3P_1$  metastable state and two atoms in the  $M_J = 0$  substate (no depolarization occurs in the excited state in an evacuated cell). Changes in this metastable alignment caused by collisions or resonant rf can be detected as changes in the  $^3P_1$  to  $^3P_0^o$  absorption of 3683-Å resonance radiation. The 3683-Å absorption is  $A_{3683} = (n_{-1} + n_{+1})C_{3683}I_{3683}$  using the relative transition probabilities in Fig. 7;  $n_{M_J}$  is the density of the  $M_J$  substate of the  $^3P_1$  state,  $C$  is a constant which converts a relative transition probability into an absolute probability, and  $I_{3683}$  is the intensity of 3683-Å light. In the simple example of the four atoms  $A_{3683} = 2C_{3683}I_{3683}$ . Upon saturation with resonant rf,  $n_{-1} = n_{+1} = \frac{4}{3}$  and  $A'_{3683} = \frac{8}{3}C_{3683}I_{3683}$ . The signal or change in absorption upon application of the rf is  $A'_{3683} - A_{3683} = \frac{2}{3}C_{3683}I_{3683}$ , which is positive, i.e., the absorption increases at resonance. This was observed as in Fig. 8(a). The  $^3P_1$  resonance can also be seen as a change in the absorption of 3640-Å light:  $A_{3640} \propto n_{-1} + n_{+1} + 2n_0$  (the  $^3P_1 \rightarrow ^3P_1^o$  probabilities can be obtained from the  $^3P_1 \rightarrow ^3P_1^o$  probabilities in Fig. 7). Then  $A'_{3640} - A_{3640} = (\frac{16}{3} - 6)C_{3640}I_{3640} = -\frac{2}{3}C_{3640}I_{3640}$ , i.e., the absorption decreases at resonance as was observed [Fig. 8(b)]. This simple calculation also predicts the ratio of signal strengths if the ratios of the two intensities of absorbable light and the absorption constants are known. The  $LS$  identification is used for convenience, but no choice of coupling schemes is necessary since  $J$  (or  $F$  in  $\text{Pb}^{207}$ ) is a good quantum number in weak magnetic fields. All of the metastable signals have the predicted signs.

These  $\text{Pb}^{208}$  signals have been observed in several ways: the  $^3P_1$  resonance by transmission of 2833-, 3640-, or 3683-Å light and by fluorescence at 2833 or 3683 Å; the  $^3P_2$  by 2833- or 4058-Å [Fig. 8(c)] transmission and 2833-, 3640-, 3683-, or 4058-Å fluorescence. All signals disappear when only 2833-Å light reaches the cell. All  $^3P_2$  signals vanish if the 4058-Å pumping light is removed.

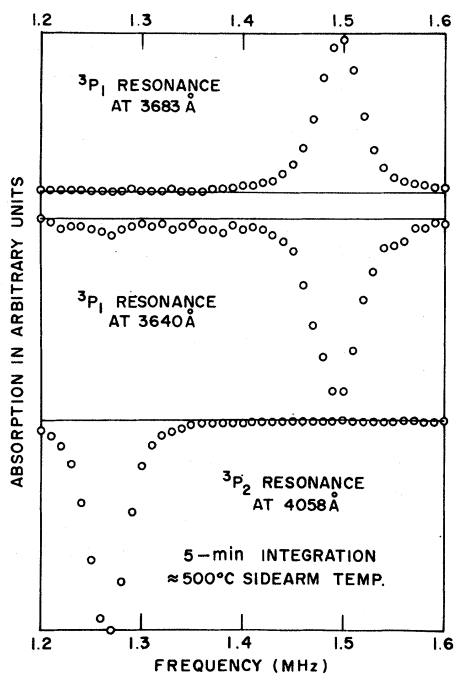


FIG. 8. Optical pumping in  $\text{Pb}^{208}$  with unpolarized light in a magnetic field of almost 0.71 G.

The branching ratio from the  $^3P_1^o$  excited state is about 20 to 30% to each of the  $^3P_1$  and  $^3P_2$  states but less than 1% to the  $^1D_2$  (accompanied by 7229-Å fluorescence).<sup>7</sup> The  $^1D_2$  alignment is monitored by the absorption of unpolarized 3573-Å light from the same lamp. The 3573-Å output is much weaker than the lines absorbed by the  $^3P_1$  and  $^3P_2$  states. In spite of these difficulties, reasonably good signal-to-noise ratios have been achieved with averaging (see Fig. 9). The claim in Ref. 3 that this is the first optical pumping of a state with  $L > 1$  is re-

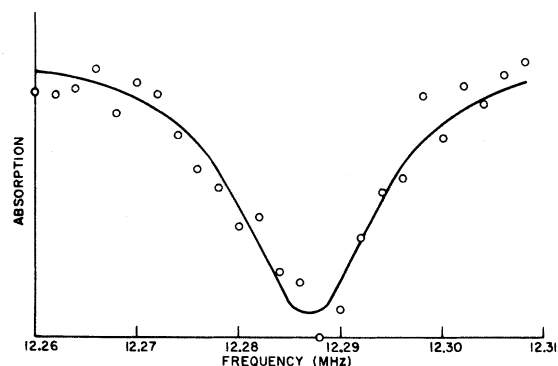


FIG. 9. Optical pumping of the  $^1D_2$  metastable state of  $\text{Pb}^{208}$  with unpolarized light. The integration time was about 15 min.

stricted to closed cells; previous work had been reported in atomic beams.<sup>14</sup>

The signals described above employing unpolarized light are alignment signals. Pumping with circularly polarized light establishes in the metastable state an orientation in addition to an alignment. If the light used to monitor the metastable polarization is also circularly polarized, the signal has contributions from the alignment and the orientation. The observed 4058-Å unpolarized and circularly polarized signals are of opposite sign and the 3683-Å signals of the same sign, in agreement with calculation. In  $\text{Pb}^{208}$  the unpolarized and circularly polarized signals are comparable, the increased efficiency of circularly polarized pumping being roughly offset by the 30 to 35% transmission of the linear polarizer.

The calculation of signal strengths and signs is more complicated for  $\text{Pb}^{207}$  ( $I = \frac{1}{2}$ ) but has been carried out assuming no ground-state polarization and lamp hyperfine components in the ratio of theoretical transition probabilities. But again the signs agree with the experimental results; early resonances are shown in Fig. 10. The  $\text{Pb}^{207}$  signals are much smaller than for  $\text{Pb}^{208}$ . This is drama-

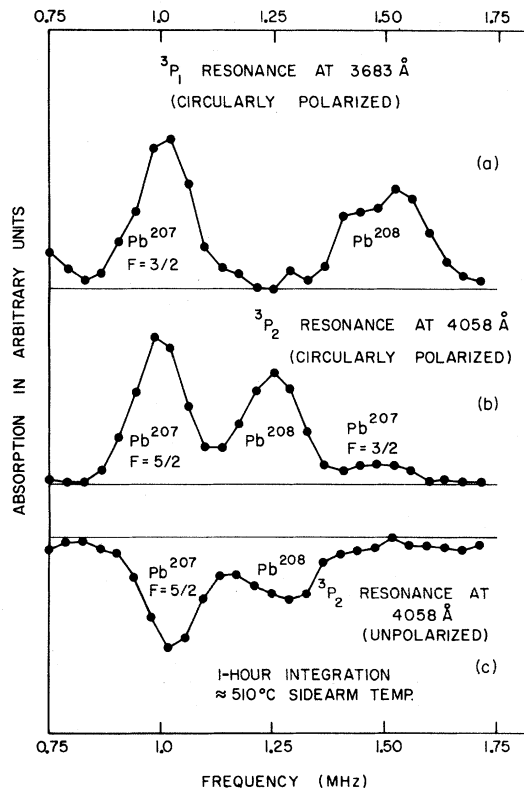


FIG. 10. Optical pumping in  $\text{Pb}^{207}$  in a field of about 0.71 G.

tized by the fact that the 7.6%  $\text{Pb}^{206}$  and  $\text{Pb}^{208}$  in the sample give a signal comparable to that from the 92.4%  $\text{Pb}^{207}$ ; this is convenient for magnetic field calibration. The ratio of  $\text{Pb}^{207}$  and  $\text{Pb}^{208}$  unpolarized 4058-Å signals decreased from 10:1 to 1:2 with an increase in sidearm temperature from about 450 to 550 °C.

$\text{Pb}^{207}$  has nuclear spin  $I = \frac{1}{2}$  and strong hyperfine interactions.<sup>15</sup> Therefore, in the linear Zeeman region we find

$$g_F \approx \frac{g_J[F(F+1) + J(J+1) - I(I+1)]}{2F(F+1)}.$$

Resonances in both hyperfine states of the  $^3P_1$  and  $^3P_2$  states were observed at the expected frequencies. The 3640-Å  $^3P_1$  resonances are weaker than those at 3683 Å; only the latter will be discussed here. The  $^3P_1$ , 3683-Å,  $F = \frac{3}{2}$  circularly polarized pumping resonance is observed easily [see Fig. 10(a)]. To verify that this signal was not simply a  $^3P_2$ ,  $F = \frac{5}{2}$  resonance (which is in near coincidence), a Corning 7-54 filter was inserted into the pumping beam. Its transmission at 2833, 3683, or 4058 Å is roughly 80, 80, or 7%, respectively. The signal was reduced by slightly more than a factor of 2—much less than for a spurious  $^3P_2$  resonance, which must be detected with 4058-Å light. The somewhat smaller 3683-Å,  $F = \frac{3}{2}$  unpolarized signal has also been observed by integrating for a few hours.

In the  $^3P_1$ ,  $F = \frac{1}{2}$  level, the alignment (and hence the unpolarized signal) is zero, of course. The

3683-Å,  $F = \frac{1}{2}$  circularly polarized signal, expected to be down by 19 from the corresponding  $F = \frac{3}{2}$  signal, has been observed after several hours of integration.

Both 4058-Å  $^3P_2$  circularly polarized pumping resonances are shown in Fig. 10(b); the expected ratio of  $F = \frac{5}{2}$  to  $F = \frac{3}{2}$  circularly polarized signals is 5.9. With unpolarized pumping, only the  $F = \frac{5}{2}$  resonance was detected [Fig. 10(c)]; the predicted ratio of  $F = \frac{5}{2}$  to  $F = \frac{3}{2}$  unpolarized signals is 56. Then for  $I \neq 0$  isotopes, circularly polarized pumping is often preferred over unpolarized pumping. Also the larger  $F$ , the larger the signal.

### B. Apparatus

A block diagram of the apparatus is shown in Fig. 11. Most of the components are described in Paper I.<sup>1</sup> Insertion of a linear polarizer and stressed-quartz quarter-wave plate between the lamp and cell produced elliptically polarized light at both the pump (2833 Å) and detection wavelengths and permitted observation of orientations. An rf modulation frequency of 1 kHz was typical in the lock-in detection mode.

A PAR waveform educator was used instead of the boxcar for early alignment transients and was often used to monitor the signal strength even when the boxcar and long-term integrator were used to improve the signal-to-noise ratio. The educator is not well suited to long integrations since different electrical components sample different portions of

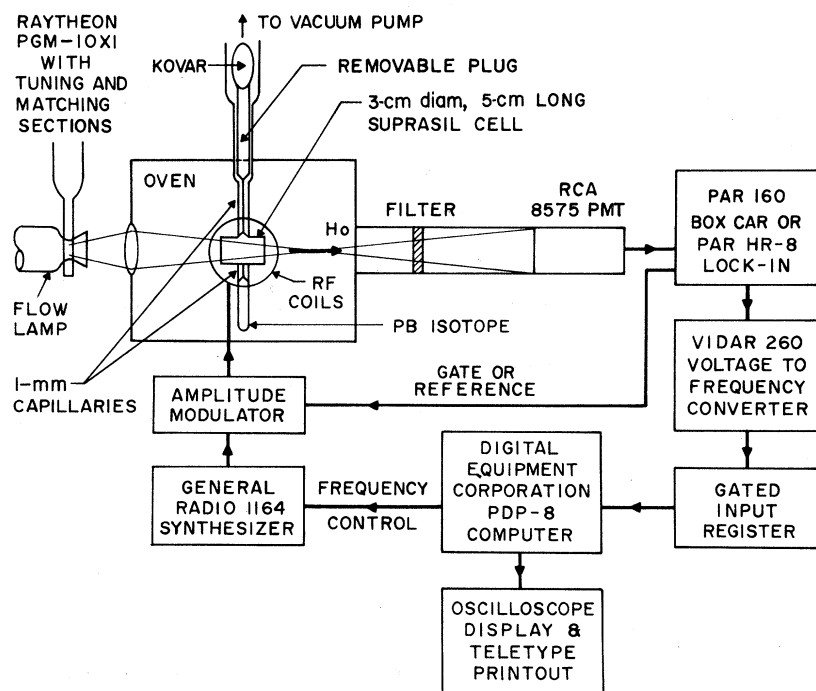


FIG. 11. Block diagram of the optical pumping apparatus for the Pb metastable states.



the transient, and these components can never be matched exactly. Data accumulation is slower with the boxcar but can be continued indefinitely to suppress noise.

A Barocel capacitance manometer with 0–1000- and 0–10-Torr sensors (the most sensitive scale on the latter sensor was 1-mTorr full scale) simplified pressure measurements.

#### C. $^1D_2$ , $^3P_2$ , and $^3P_1$ $g_J$ Values

Measurements of the  $g_J$  values of the metastable states were made by determining ratios. The ratio  $g_J(^3P_1)/g_J(^3P_2) = 1.17698(15)$  was obtained by determining the frequencies of the two alignment resonances six times each at one field value (about 50 and 42.5 MHz) and three times each at a lower field (about 15 and 12.8 MHz).<sup>16</sup> The value  $g_J(^1D_2) = 1.2263(1)$  of Lurio and Landman<sup>14,15</sup> then gives  $g_J(^3P_2) = 1.2753(4)$  and  $g_J(^3P_1) = 1.5010(5)$  where the quoted errors are three standard deviations of the mean.

At the time of the  $g_J$  measurements the author was unaware of the Lurio and Landman measurement of  $g_J(^1D_2)$ . Therefore, an absolute calibration of the field was made via eight determinations (42.5 MHz and 18 kHz) of the ratio

$$\frac{g_J(\text{Pb } ^3P_2)}{g_J(\text{Hg } ^{199}\text{ } ^1S_0)} = \frac{(\nu_{\text{Pb}}/\nu_{\text{Hg}})}{(\mu_B/\mu_N)} = \frac{\nu_{\text{Pb}}}{1836.1\nu_{\text{Hg}}} = 1.2800(13),$$

where  $\mu_B$  and  $\mu_N$  are the Bohr and nuclear magnetons, respectively. The Hg ground state was optically pumped with circularly polarized light in the same cell permitting rapid alternations between the Hg nuclear resonance and Pb electronic resonance as in Ref. 1. The assigned error is about 7.5 times the standard deviation of the mean. This 0.1% error is included for the following reason: There is almost complete motional averaging in the Hg case, so its frequency corresponds to the average field in the cell. But a Pb metastable state is depolarized by a single wall collision (see Sec. IIIE). With 50% or so absorption most of the signal comes from the front portion of the cell. Also the Pb-lamp spatial profile may not have been uniform. Field measurements with an NMR probe showed that the gradient across the cell was certainly less than 0.1% and that the average field seen by the Pb was more than likely less than that seen by the Hg. At any rate the 0.1% error is conservative. With  $\mu_I(\text{Hg } ^{199}) = 0.497865(6)\mu_N$  from Cagnac,<sup>17</sup> one obtains  $g_J$  values consistent with the more precise ones given above. The ratios used in the determination of those values should be independent of spatial-nonuniformity and field-inhomogeneity uncertainties. This is because the same lamp was used for all the Pb resonances, and the average field seen by the three states should have been the same.

#### D. $^3P_1$ and $^3P_2$ Disalignment Cross Sections and Ratios in Pb<sup>208</sup>

The cross sections were determined by measuring the optical-pumping recovery time of the metastable signal after the removal of resonant rf which destroys the alignment. For unpolarized pumping and detecting light along the field, the apparent-pumping time  $\tau$  is given by

$$\frac{1}{\tau} = \frac{1}{T_w} + (\sigma_A + \sigma_Q)n\bar{v} + \frac{1}{T_R} + \frac{1}{T_P}, \quad (23)$$

where  $T_w$  is the time for relaxation by wall collisions;  $\sigma_A$  and  $\sigma_Q$  are the cross sections for disalignment and quenching, respectively, in collisions at relative velocity  $\bar{v}$  with foreign-gas atoms of density  $n$ . It is shown in the Appendix that under these conditions that the transients monitor only an alignment; relaxation of other multipole moments does not enter.  $T_R$ , the radiative decay time ( $>10$  msec),<sup>18</sup> and  $T_P$ , the optical-pumping time ( $>10$  msec), were both negligible compared with  $T_w$  which was less than 50  $\mu\text{sec}$  for the  $^3P_1$ ,  $^3P_2$ , and  $^1D_2$  states. The  $^1D_2$  signal was too small for studying foreign-gas relaxation. The  $^3P_1$  and  $^3P_2$  apparent-pumping times ranged from 40  $\mu\text{sec}$  at 0 Torr to 15  $\mu\text{sec}$  for something less than  $10^{-2}$  Torr. At these low pressures, excited-state disalignment (see Sec. II) is negligible because of the much shorter excited-state lifetime, even though the cross sections are comparable to those in the metastable states. It will be shown in Sec. IV that the quenching cross sections are negligible compared to the disalignment cross sections. Then to an excellent approximation we find that

$$1/\tau \approx 1/T_w + \sigma_A n\bar{v}. \quad (24)$$

Experimentally the optical-pumping recovery transients were recorded by averaging the output of a PAR 160 boxcar (see Fig. 11) for about 15 min (see Fig. 12). The digital output was then plotted with asymptote subtracted on semilog paper and the value of  $\tau$  extracted from an eyefit straight line through the points (see Fig. 13). Values of  $1/\tau$  and pressure (or  $n$ ) were then assigned 10% errors as a conservative overestimate of data scatter and least squares fitted to a straight line (Fig. 14). The computer output included best-fit values of  $T_w$  and  $\sigma_Q$ , their standard deviations, and their standard deviations of external consistency.

There was one complication to these very straightforward alignment cross-section measurements. The cell temperature  $T_C$  was almost three times hotter than the pressure gauge at room temperature  $T_G$ . At high pressures the cell pressure  $P'_C$  is the same as the gauge pressure  $P'_G$  to balance forces since wall collisions are negligible. At low pressures, gas collisions are negligible; in equilibrium the transport must vanish requiring  $n_C v_C$

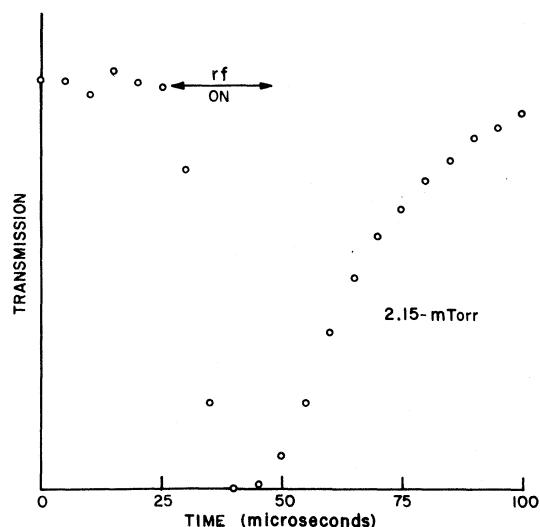


FIG. 12.  $\text{Pb}^{208} \text{}^3\text{P}_1$  optical-pumping recovery transient with 2.15 mTorr of He after application of resonant rf. The photomultiplier output was amplified by a PAR CR-4 low-noise amplifier (LO-Z DIFF input, 100-Hz low cutoff, 300-kHz upper cutoff,  $10^3$  gain), averaged by a PAR 160 boxcar (1.5- $\mu\text{sec}$  prefilter, 2.5- $\mu\text{sec}$  aperture, 0.1-sec time constant), and further averaged for 250 cycles by a computer averager (0.2 sec per channel).

$=n_G v_G$  or  $P'_C = P'_G (T_C/T_G)^{1/2}$ . The pressures 1–8 mTorr used in this experiment lie in the transition region between these two extremes. The cross sections reported in Ref. 3 are in error because it was incorrectly assumed that  $P'_C = P'_G$ . Since then corrections  $C$  have been determined experimentally,

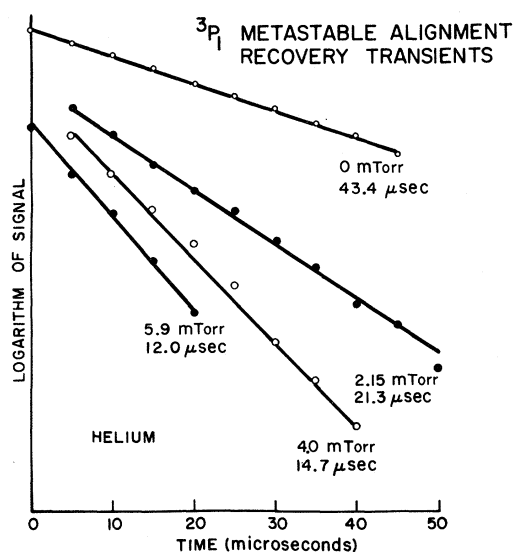


FIG. 13. Determination of apparent pumping times  $\tau$  from the exponential recovery transients.

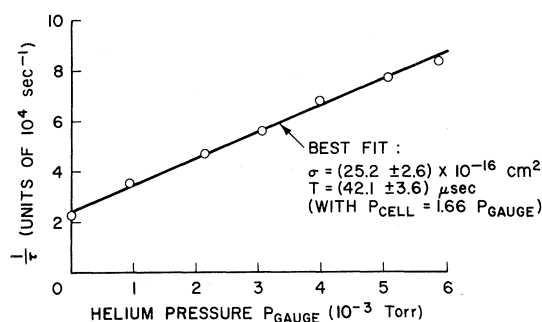


FIG. 14. Determination of the cross section for disalignment of the  $\text{Pb}^{208} \text{}^3\text{P}_1$  metastable state by a least-squares fit of  $\tau^{-1} = T^{-1} + \sigma n$ .

which relate the gauge pressure  $P'_G$  to the high-temperature cell pressure  $P'_C$ ; i.e.,  $P'_C = C P'_G$ . This was done by attaching the manometer to a room-temperature volume  $V_G$  comparable to the cell volume  $V_C$  but separated from the cell and from the vacuum line by stopcocks. With the entire system (including the cell) at room temperature,  $V_C$  and  $V_G$  were evacuated, the valve between them closed,  $V_G$  filled to high pressure  $P_G$ , and the valve opened reducing the pressure to  $P'_G$ , then  $V_C/V_G = P_G/P'_G - 1$ . With the cell at high temperature the process was repeated for various pressures as shown in Fig. 15. The number of atoms initially in  $V_G$  was the constant in the experiment:

$$N_G = N'_G + N'_C = \frac{P'_G V_G}{k T_G} + \frac{P'_C V_C}{k T_C} = \frac{P_G V_G}{k T_G}, \quad (25)$$

$$\frac{P'_C}{P'_G} = \frac{V_G}{V_C} \frac{T_C}{T_G} \left( \frac{P_G}{P'_G} - 1 \right) \equiv C. \quad (26)$$

Actually, further refinements were made to correct for the fact that the sidearm and connecting tube were at different temperatures.  $C$  depends upon the

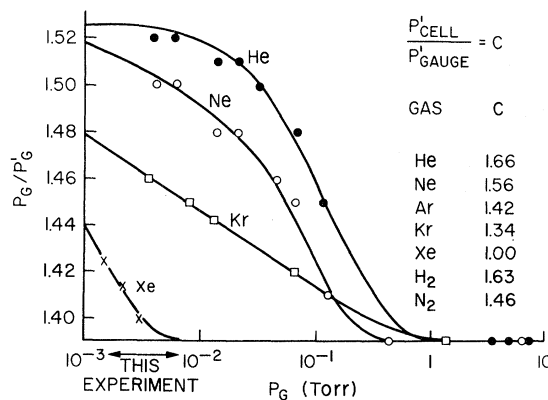


FIG. 15. Data used to determine the correction to the gauge pressure to obtain the pressure in the cell at elevated temperature (see text).

TABLE II. Values of the disalignment cross sections for the  $^3P_1$  and  $^3P_2$  metastable states of  $\text{Pb}^{208}$ . When the uncertainties in the pressure corrections are included at 813 °K, these values should be accurate to  $\pm 20\%$ . The ratio uncertainties are as listed.

	$\frac{\sigma_A(^3P_1)}{(\text{\AA}^2)}$	$\frac{\sigma_A(^3P_2)}{(\text{\AA}^2)}$	$\frac{\sigma_A(^3P_2)}{\sigma_A(^3P_1)}$	
				Alternation at one pressure      All data
He	$27.06 \pm 1.88$	$36.07 \pm 2.45$	$1.26 \pm 0.11$	$1.33 \pm 0.13$
Ne	$27.30 \pm 2.04$	$35.48 \pm 3.60$		$1.30 \pm 0.16$
Ar	$50.60 \pm 3.73$	$59.12 \pm 5.91$	$1.19 \pm 0.11$	$1.17 \pm 0.15$
Kr	$63.59 \pm 8.75$	$76.12 \pm 6.35$		$1.20 \pm 0.19$
Xe	$122.82 \pm 17.0$	$159.31 \pm 13.44$	$1.16 \pm 0.11$	$1.30 \pm 0.21$
$\text{H}_2$	$26.39 \pm 2.51$	$38.78 \pm 4.02$		$1.47 \pm 0.21$
$\text{N}_2$	$72.61 \pm 5.56$	$87.53 \pm 8.36$	$1.19 \pm 0.11$	$1.21 \pm 0.15$

pressure used; as stated above at high pressures  $C=1$  and at low pressures

$$C \approx (T_c/T_g)^{1/2} \approx (813/295)^{1/2} = 1.66.$$

In this experiment the pressures usually ranged between 2 and 8 mTorr;  $C$  was taken to be constant over this small range and equal to the values listed in Fig. 15. Xe was approximately in the high-pressure limit and He in the low; the others were in the transition region. The cross-section error resulting from the uncertainty in  $C$  and the temperature measurement should not exceed 15%. In Table II are listed the best-fit values of the  $^3P_1$  and  $^3P_2$  disalignment cross sections; the errors include only statistical errors arising from the assumed  $\pm 10\%$  uncertainties in  $\tau^{-1}$  and  $P$  or, in the case of the Xe  $^3P_1$  cross section, from an external consistency uncertainty from three measurements. Since these uncertainties are about  $\pm 10\%$ , the cross sections are probably accurate to within  $\pm 20\%$ , with the possibility of error in  $C$  included.

Ratios of disalignment cross sections have been determined to  $\pm 10\%$  by alternating between the  $^3P_1$  and  $^3P_2$  resonances at a fixed pressure and are listed in Table II.

#### E. Wall Disalignment

By integrating for 10 h, a zero-pressure recovery transient of the  $^1D_2$  state at 3573 Å was obtained yielding  $T_w(^1D_2) \approx 33 \pm 11 \mu\text{sec}$ . Ten measurements at 4057 Å and twelve at 3683 Å gave  $T_w(^3P_2) = 41.0 \pm 0.4 \mu\text{sec}$  and  $T_w(^3P_1) = 49.0 \pm 1.1 \mu\text{sec}$ , respectively, where the errors are standard deviations of external consistency. The ratio is then

$$T_w(^3P_1)/T_w(^3P_2) = 1.195 \pm 0.029. \quad (27)$$

These relaxation times contained no appreciable contribution from the pumping radiation since they did not change with a factor-of-6 reduction in light intensity. The sidearm controlling the Pb density was usually about 500 °C implying a density of about  $1.6 \times 10^{11} \text{ cm}^{-3}$  or about two absorption lengths in the cell. A nonuniform initial distribution may be responsible for the difference between the observed values and that calculated from a uniform distribution and complete depolarization with every wall collision  $T = 4V/(\bar{v}S) = 77 \mu\text{sec}$ , where  $V$  and  $S$  are the volume and surface area of the 3-cm-diam 5-cm-long cell. For more discussion see Sec. VB.

#### IV. QUENCHING OF $^3P_1$ METASTABLE STATE BY FOREIGN-GAS COLLISIONS

Collisional destruction of the  $^3P_1$  metastable state was observed as follows (see Figs. 1 and 16). The metastables were produced by 2833-Å excitation to the  $^3P_1^o$  excited state followed by spontaneous decay

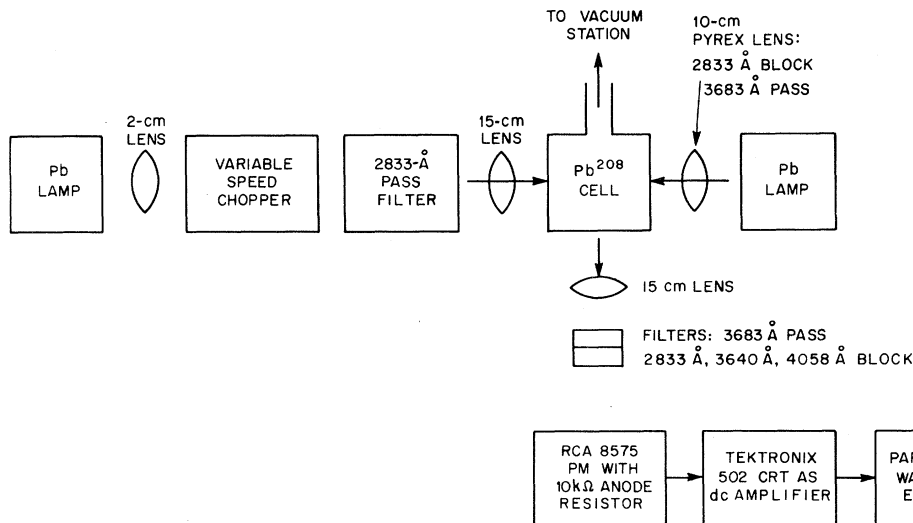


FIG. 16. Apparatus for measuring the lifetime of the  $\text{Pb } ^3P_1$  metastable state in the presence of various foreign gases. The 2833-Å pass filter was a nickel sulfate liquid filter; the other filters were interference filters.

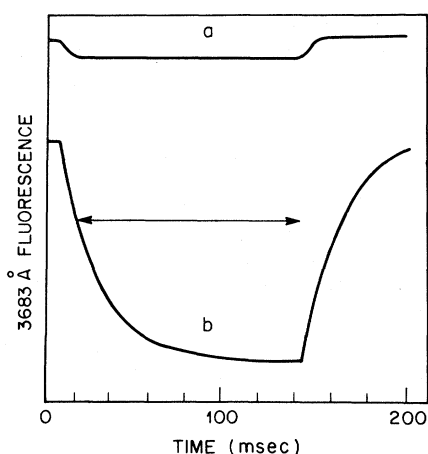


FIG. 17. Curve a: 3683-Å fluorescence signal with the 3683-Å beam blocked. This leakage signal shows the time dependence of the pumping beam. A slit at the chopper limits the on-to-off time to 10% or less of the off time. Curve b: 3683-Å fluorescence signal with the 3683 Å beam on. Only the decay of the fluorescence with the pumping radiation off (between the arrowheads) was used in determining the lifetime. These data were taken with 300 Torr of Xe and using a PAR TDH-9 waveform eductor.

to the  $^3P_1$  state. The metastable density was monitored by 3683-Å fluorescence arising from the metastable absorption of 3683-Å radiation from a second lamp. Note that absorption of the 3683-Å radiation does not change the density of metastable so long as quenching of and excitation transfer from the  $^3P_0$  state are negligible. The 2833-Å production radiation was suddenly removed by the chopper, and the decay of the metastable density was monitored by the 3683-Å fluorescence. Any reflected 3683-Å light appeared as a dc background. Any 3683-Å radiation from the pump light was, of course, cut off by the chopper. Similar metastable-lifetime measurements have been made in Tl, placing a lower limit of 4 msec on the Tl  $^2P_{3/2}$  metastable lifetime.<sup>19</sup>

It was established very early from the disalignment cross sections of Table II that the  $^3P_1$  state

TABLE III. Cross sections (in  $10^{-20}$  cm<sup>2</sup>) for quenching of the Pb  $6p^2$   $^3P_1$  and  $^3P_2$  metastable states by foreign gases.

Quencher	$\sigma_Q(^3P_1)$	$\sigma_Q(^3P_2)$
He	<0.003	<0.01
Ne	<0.006	<0.01
Ar	<0.04	
Kr	<0.02	
Xe	<0.04	
N <sub>2</sub>	≤0.13	<0.3
H <sub>2</sub>	24 ± 5	
D <sub>2</sub>	≤0.3	

is completely disaligned at the pressures (>1 Torr) used in the quenching studies. No rf was then needed to disalign the state and ensure that the transient was a decay of the population alone ( $L=0$  multipole only; see the Appendix). The fact that these metastable states live longer than their alignment resulted in much larger lifetime than disalignment signals. Consequently, a waveform eductor sufficed for the lifetime measurements.

Figure 17 displays a tracing of a representative metastable decay curve, and Fig. 18 presents various quenching curves taken by this method. Ar, Kr, and N<sub>2</sub> showed less pressure dependence: 8 to 18 msec, 25 to 400 Torr; 15 to 35 msec, 25 to 400 Torr; 4 to 8 msec, 20 to 250 Torr, respectively. From these data, values or upper limits were determined for the quenching cross sections (at 540 °C) except for D<sub>2</sub> at 600 °C) and are listed in Table III. No distinction is made between quenching directly to the ground state and destruction via another metastable state. It was not shown that the Xe quenching may not have been an impurity in the Xe; a dry-ice trap was used for Kr and Xe rather than liquid nitrogen as in the other cases. In the D<sub>2</sub> run the zero-pressure datum point implies

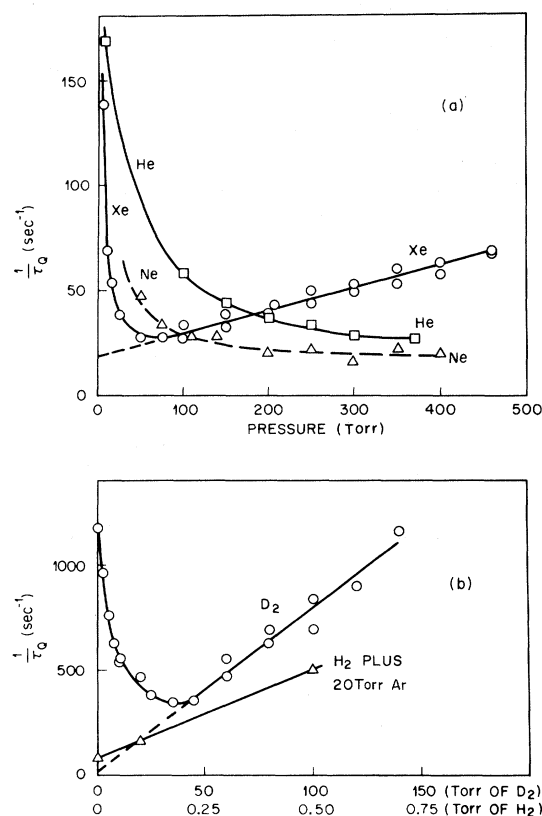


FIG. 18. Lifetime  $\tau_Q$  of the Pb  $^3P_1$  metastable state for various foreign-gas pressures.

a metastable lifetime of 850  $\mu\text{sec}$ —16 times the disalignment time and 11 times the calculated time between wall collisions (see Sec. III E). Therefore, the  $^3P_1$  metastable state survived several wall collisions before being destroyed.<sup>20</sup>

The value  $\tau \approx 55$  msec found for 400 Torr of Ne is a lower limit for the radiative lifetime. It also agrees with the lifetime value from extrapolation of the high-pressure Xe data. It was determined that the measured lifetimes were independent of the intensity of 3683-Å monitoring beam and the diameter of an aperture placed at the lens between the chopper and cell. The operating temperature of the sidearm was about 500 °C implying a density of about  $1.6 \times 10^{11} \text{ cm}^{-3}$ ; no quenching was expected from Pb-Pb collisions at this density, but no careful check was made to verify this. The  $1/\tau$  values for high Xe pressures must be determined by radiative decay and gas collisions since diffusion to the walls is negligible. The  $^3P_1$  radiative lifetime must then be  $53 \pm 30$  msec, where the uncertainty is a standard error<sup>21</sup> as determined by a least-squares fit of the Xe data for pressures of 200 Torr and above, assuming a 5% uncertainty in each pressure measurement and a 20% uncertainty in each reciprocal lifetime. The standard deviation of external consistency<sup>21</sup> is four times smaller. There is no doubt that this measured lifetime is a lower limit to the radiative lifetime. In the absence of another explanation for this apparent limit on the lifetime, it is offered as the radiative lifetime. It compares with 137 msec calculated by Garstang.<sup>18</sup>

For 400 Torr of Ne and assuming a Pb-Ne kinetic cross section of  $10^{-16} \text{ cm}^2$  the metastable undergoes about  $10^7$  collisions per sec with the Ne or almost a million collisions in its 55-msec lifetime. Thus even though the alignment of the  $^3P_1$  metastable state is destroyed by a minuscule (few mTorr) quantity of foreign atoms, the state itself is highly resistant to deexcitation.

The factor of 100 between the  $\text{H}_2$  and  $\text{D}_2$  values in Table III is striking. The  $\text{D}_2$  value may even be lower since there could have easily been a 1% impurity of  $\text{H}_2$  in the  $\text{D}_2$ . The  $\text{H}_2$  data were taken with 20-Torr Ar because the larger  $\sigma_0$  prevents any lengthening of the lifetime by reduced diffusion to the walls. A few hours were required for the completion of the mixing of the  $\text{H}_2$  and Ar and stabilization of the measured lifetime.

The quenching method was also applied to the  $^3P_2$  metastable states, yielding the results shown in Table III and a lower limit of the radiative lifetime of 40 msec (expected to be almost 3 sec).<sup>18</sup> Experimentally the situation is more difficult than for the  $^3P_1$  state. In the latter case 3683-Å fluorescence resulting from 3683-Å absorption monitored the metastable density. No 3683-Å radiation arose from the 2833-Å pumping beam either by reflection (since the

filter blocked 3683-Å light) or by fluorescence (since the  $^3P_0$  state is not excited by the pumping beam). In the  $^3P_2$  case, 4058-Å fluorescence from absorption of a dc 4058-Å lamp indicated the  $^3P_2$  density. But there was a large background of modulated 4058-Å fluorescence from the modulated excitation of the  $^3P_1^o$  excited state. This background was zero during the decay half-cycle since the exciting beam was off, but it could saturate the sensitive amplifiers during the other half-cycle. Clearly the detector could be gated or a second chopper synchronized to eliminate this background and permit measurements in the  $^3P_2$  state comparable to those described for the  $^3P_1$  state. In particular it would be interesting to see how large a lower limit could be placed on the radiative lifetime and to measure the  $\text{H}_2$  and  $\text{D}_2$  quenching cross sections.

## V. COMPARISON WITH THEORY

### A. Theoretical Values of Total Disalignment Cross Sections

Many papers treating the effects of foreign-gas collisions on line shapes and relaxation rates are referenced by Berman and Lamb.<sup>22</sup> A comparison is made here with the results of Omont.<sup>23</sup> The interaction is assumed to be purely electrostatic and of sufficiently long range to permit a multipole expansion. The lowest-order term contributing to a nonresonant collision is the second-order induced dipole-induced dipole; higher-order terms are ignored. The internal states of the atoms are treated quantum mechanically, but the relative position is assumed to be a classical straight-line trajectory. In a perturbation treatment of the scattering process, Omont then finds for the average nonresonant cross section for disalignment of a  $J=1$  state by a  $^1S_0$  perturber:

$$\sigma_A = (v \sigma_{NR}^{aI})_{av} / v_{av} = C(\beta' / \Delta E)^{2/5} (v^{3/5})_{av} / v_{av} . \quad (28)$$

A lower limit of 1.8 is obtained for  $C$  by assuming the calculated dependence upon impact parameter is valid even for vanishing impact parameter and should be a good approximation for large cross sections (heavy-rare-gas disalignment of Pb). An upper limit of 2.7 obtains by assuming unit probability for disalignment for "strong" collisions and should be better for small cross sections (disalignment of Pb by helium and light rare gases). By numerical integration of the Schrödinger equation and over impact parameters, Berman and Lamb<sup>22</sup> found  $C = 2.52$ ; their value is used in calculating the  $^3P_1$  cross sections below. The relative velocity is  $v$ , and the averages are over the velocity distribution.  $\Delta E$  is an appropriate average in the Unsöld approximation of the difference between the intermediate-state energy of the perturbed and perturbing atoms and the energy of their initial states. This average which permits closure and

simplification of the second-order perturbation matrix elements should be a reasonably good approximation in Pb and the rare gases where a few strong dipole transitions dominate. The remainder of the atomic structure details reside in the factor  $\beta'$ :

$$\beta' = P_2^2 \langle J0 | P_1^2 - 3P_{1z}^2 | J0 \rangle / J(J+1) = P_2^2 \alpha, \quad (29)$$

where

$$P_2^2 = e^2 \langle S_0 | \left| \sum_i \vec{r}_{2i} \right|^2 | S_0 \rangle.$$

is the mean square of the electric dipole of perturbing atom labeled 2 (the sum is over the electrons of the perturber, and  $\vec{P}_1 = e \sum_j \vec{r}_{1j}$  is the electric dipole of the electrons of the perturbed atom labeled 1.

For Pb the calculation of  $\alpha$  for two-electron states is of interest. One then has for electrons  $a$  and  $b$

$$P^2 - 3P_z^2 = D + E, \quad (30)$$

where

$$D = -2 \left( \frac{4}{5} \pi \right)^{1/2} [r_a^2 Y_{20}(\Omega_a) + r_b^2 Y_{20}(\Omega_b)] e^2 \quad (31)$$

and

$$E = + \frac{8}{3} \pi r_a r_b [\sum_m Y_{1m}^*(\Omega_a) Y_{1m}(\Omega_b) - 3Y_{10}(\Omega_a) Y_{10}(\Omega_b)] e^2, \quad (32)$$

utilizing Table 1 of Edmonds.<sup>24</sup> The cross terms vanish except for an antisymmetrized state, where  $a$  and  $b$  have opposite parity. If  $Q$  is an antisymmetrizing operator and  $P_{ab}$  an interchange operator, an arbitrary antisymmetrized state  $|J0\rangle$  can be written in terms of unsymmetrized states  $|j_a m_a\rangle$  and  $|j_b m_b\rangle$ :

$$|J0\rangle = Q|\psi\rangle = Q \sum_{m_a, m_b} \langle j_a m_a j_b m_b | J0 \rangle |j_a m_a\rangle |j_b m_b\rangle, \quad (33)$$

where

$$Q = [1 - (-)^{j_a + j_b - J} P_{ab}] / \sqrt{2} \quad (34)$$

since

$$\langle j_a m_a j_b m_b | J0 \rangle = (-)^{j_a + j_b - J} \langle j_b m_b j_a m_a | J0 \rangle.$$

$Q$  commutes with  $P^2 - 3P_z^2$  since the latter is invariant under interchange. Then we find

$$\begin{aligned} \langle J0 | P^2 - 3P_z^2 | J0 \rangle &= \langle \psi | Q(P^2 - 3P_z^2)Q | \psi \rangle \\ &= \langle \psi | (P^2 - 3P_z^2)Q^2 | \psi \rangle \\ &= \sqrt{2} \langle \psi | (P^2 - 3P_z^2)Q | \psi \rangle \end{aligned} \quad (35)$$

since  $Q^2 = \sqrt{2}Q$ . Then we find

$$\alpha = \frac{\langle J0 | D | J0 \rangle - (-)^{j_a + j_b - J} \langle j_a j_b J0 | E | j_b j_a J0 \rangle}{J(J+1)}, \quad (36)$$

where the  $D$  and  $E$  matrix elements can be calcu-

lated using Edmonds<sup>24</sup> without further concern for antisymmetrization.

### 1. Calculation of $\sigma_A(^3P_1)$

For Pb,  $jj$  coupling is almost exact.<sup>25</sup> For the  $^3P_1$  state in the  $6p^2$  configuration any coupling scheme is equivalent since there is no other state with  $J=1$ . But  $jj$  coupling is used here since it should be used in the  $^3P_2$  state. The  $^3P_1$  state is constructed with  $j_a = \frac{1}{2}$  and  $j_b = \frac{3}{2}$ . Since  $a$  and  $b$  have the same parity, the  $E$  matrix element vanishes. The  $D$  matrix element is calculated in the standard way: the Wigner-Eckart theorem [Edmonds's (5.4.1)]

$$\begin{aligned} \langle j_a j_b J | Y_2(\Omega_a) | j_a j_b J \rangle &\propto \langle l_a s_a j_a | Y_2(\Omega_a) | l_a s_a j_a \rangle \\ &\propto \langle l_a | Y_2(\Omega_a) | l_a \rangle \end{aligned}$$

by two applications of Edmonds's (7.1.7), with (5.4.5) giving the last reduced matrix element. One finds  $\alpha = -\frac{1}{5} e^2 (r_{6p}^2)_{av}$ , where  $(r_{6p}^2)_{av}$  is the mean of the squared distance of a  $6p$  electron from the Pb nucleus.

Crude estimates of  $(r_{6p}^2)_{av}$  and  $P_2^2$  are obtained using the Slater radial functions<sup>26</sup> as approximations to the actual functions:

$$R(r) \propto r^{n^*-1} e^{-rZ^*/n^*}, \quad (37)$$

where  $n^*$  is the effective shell quantum number and  $Z^*$  is the effective charge.  $n^* = 1, 2, 3, 3.7, 4.0, 4.2$  for  $n = 1, 2, 3, 4, 5, 6$ . For an  $s$  or  $p$  shell  $Z^* - 1$  is the sum of 0.15 times the number of electrons in the next inner shell, 0.65 (0.7 for  $1s$ ) times the number in the same group as the electron of interest, and the number of electrons farther out. Then for a  $6p$  electron in the  $6s^2 6p^2$  configuration of Pb,  $n^* = 4.2$  and  $Z^* = 5.65$ . Then since

$$(r^2)_{av} = a_0^2 (n^*/Z^*)^2 (n^* + \frac{1}{2})(n^* + 1), \quad (38)$$

$(r_{6p}^2)_{av} = 13.5 a_0^2$ , where  $a_0$  is the Bohr radius.  $P_2^2/e^2$  including exchange effects is found following Ref. 27 to be

$$\begin{aligned} P_2^2/e^2 &= 2(r_s^2)_{av} + 6(r_p^2)_{av} - 4(r_{sp})_{av}^2 \\ &= 4a_0^2 n^{*2} (n^* + \frac{1}{2})(n^* + \frac{3}{2})/Z^{*2} \end{aligned} \quad (39)$$

for the rare gases and  $2(r_{1s}^2)_{av}$  for He. The values taken for  $n^*$  and  $Z^*$  are, respectively, for He, Ne, Ar, Kr, Xe: 1, 1.7; 2, 5.85; 3, 6.75; 3.7, 8.25; 4.0, 8.25.

Since  $\beta'$  is determined by the values of  $\alpha$  and  $P_2^2$  just calculated, there remain only  $\Delta E$  and the velocity averages in Eq. (28) in order to estimate the cross section. By far the strongest electric dipole transitions from the  $^3P_1$  metastable state are to the  $^3P_1^o$  and  $^3P_0^o$  excited states at 3640 (3.4 eV) and 3683 Å. The strong transitions in the rare

gases are to singlet states near the ionization limit. Therefore,  $\Delta E$  is taken as 3.4 eV plus the rare-gas ionization potential. For the velocity averages one can show that for a Maxwellian distribution

$$(v^{3/5})_{\text{av}}/v_{\text{av}} = 0.931/(\frac{1}{2}\sqrt{\pi}v_{\text{av}})^{2/5}, \quad (40)$$

where  $v_{\text{av}}$  is the average relative velocity [Eq. (18)].

The observed and theoretical values of the cross sections are listed in rows (d) and (a) of Table IV. Row (b) lists cross-section predictions for radial integrals calculated numerically using Herman and Skillman (HS) wave functions.<sup>28</sup> The latter reduce  $(r_{6p}^2)_{\text{av}}$  from the  $13.5a_0^2$  Slater value to  $12.93a_0^2$ ; the Slater and HS values of  $P_2^2/e^2a_0^2$  are, respectively: He, 2.08, 2.46; Ne, 4.09, 5.78; Ar, 12.4, 14.5; Kr, 17.6, 19.5; Xe, 23.2, 27.0. Only electrons in the outer shell were included in the averages. Faroux has shown that for Hg the agreement with theory is improved by deducing the rare-gas contribution to  $\Delta E$  by equating experimental polarizabilities with theoretical expressions containing a closure energy.<sup>29</sup> The rare-gas energy differences to be added to the appropriate Pb difference are He, 29.88 eV; Ne, 39.36 eV; Ar, 25.8 eV; Kr, 26.57 eV; Xe, 24.63 eV. Row (c) presents the corresponding theoretical values which are in fair agreement with the observed values. At least the assumed induced-dipole-induced-dipole interaction is large enough to account for the observed cross

sections.

## 2. Comparison with Wang and Tomlinson

Wang and Tomlinson<sup>30</sup> have shown in Omont's first approximation that for arbitrary angular momentum  $j$  and multipole  $x$  the cross section is given by

$$\sigma_j^{(x)} = D\phi_j^{(x)}(v^{3/5})_{\text{av}}/v_{\text{av}}, \quad (41)$$

where  $D = (\pi p_1^2 p_2^2 / 16 \Delta E)^{2/5}$  depends upon the details of the atomic structure ( $p^2 = e^2 |\tilde{r}|^2$ ). The angular average has been carried out and buried in a geometric factor  $\phi_j^{(x)}$  which is tabulated for  $j$  values up to 8. They do not discuss the fact that  $\sigma_j^{(x)}$  is in general different for different coupling schemes. In fact they have effectively assumed a single electron where  $j=l$  for integer  $j$  and  $j=l \pm \frac{1}{2}$  for odd half-integer  $j$ . For example, for integer  $j$  their Eq. (31) is obtained by setting  $\langle j || Y_2 || j \rangle = \langle l || Y_2 || l \rangle$ , where  $l$  is the orbital angular momentum quantum number. One may generalize their results to include the  $6p^{23}P_1$  state of Pb by noting that the  $Y_{2m}$  terms in their Eq. (30) come from the time integration over the classical path of  $U_i^2(t)$  yielding  $5P_{1b}^2 + P_{1v}^2 + 2P_{1i}^2$ . If  $\vec{P}_1 = \vec{P}_{1a} + \vec{P}_{1b}$  for two electrons  $a$  and  $b$ , then the  $Y_{2m}(\theta, \phi)$  in their Eq. (30) becomes  $Y_{2m}(\theta_a, \phi_a) + Y_{2m}(\theta_b, \phi_b)$  since the cross terms vanish when  $a$  and  $b$  have the same parity. Then we see that

TABLE IV. Comparison of observed disalignment cross sections with theoretically estimated values. For the  $^3P_1$  states the constant  $C$  in Eq. (28) is taken as 2.52 as found numerically by Berman and Lamb. The two theoretical values for the  $^3P_2$  state are Omont's approximations 1 and 2. The abbreviations are as follows: RG, rare gas; S, Slater; HS, Herman and Skillman;  $E_I$ , ionization potential;  $E_D$ , effective energy found by equating a theoretical expression for the polarizability with the experimental value (Ref. 29);  $T_R$ , dipole estimated from experimental lifetime rather than from wave functions. This table illustrates the effect of various approximations. The theoretical values in the row just above the observed values should be the most reliable ones calculated here. Other evidence leads one to expect the neglected repulsive core to make the observed values for He and Ne larger than the theoretical ones (Ref. 32). The disagreement between theory and experiment is not much larger than the 20% experimental uncertainties and probably arises from the use of the crude  $\Delta E$  closure approximation. The difference between using HS wave functions is not very significant. But the use of S functions to estimate  $(r_{6p,7s})_{\text{av}}$  for  $\sigma(^6P_7)$  is grossly inaccurate. The  $\Delta E$  values used by Faroux improve the agreement as they do for Hg (Ref. 29).

	Wave function		$\Delta E$ (eV)		He	Ne	Ar	Kr	Xe
	Pb	RG	Pb	RG					
$\sigma_A(^6P_1)$ (a)	S	S	3.4	$E_I$	22	41	70	106	131
(b)	HS	HS	3.4	$E_I$	23	46	83	109	137
(c)	HS	HS	3.4	$E_D$	21	37	70	87	108
(d)		Experimental			27	27	51	64	123
$\sigma_A(^6P_2)$ (e)	S	S	3.04	$E_I$	21-27	39-50	77-97	103-131	127-161
(f)	HS	HS	3.04	$E_I$	22-28	44-56	80-102	106-134	133-169
(g)	HS	HS	3.04	$E_D$	20-25	32-40	64-82	83-104	100-127
(h)		Experimental			36	35	59	76	159
$\sigma_A(^6P_7)$ (i)	S	S	0	$E_I$	43	80	159	216	270
(j)	$T_R$	S	0	$E_I$	21	39	77	105	131
(k)	$T_R$	HS	0	$E_I$	22	44	81	107	136
(l)	$T_R$	HS	0	$E_D$	20	34	66	83	103
(m)		Experimental			28	46	73	...	105

$$\sigma_f^{(x)} = D\Phi_f^{(x)}(v^{3/5})_{av}/v_{av}, \quad (42)$$

$$\Phi_f^{(x)} = \phi_f^{(x)} \left\{ [\langle J || Y_2(\Omega_a) || J \rangle + \langle J || Y_2(\Omega_b) || J \rangle] / \left[ (-)^J (2J+1) \left( \frac{5}{2} \pi \right)^{1/2} \begin{pmatrix} J & 2 & J \\ 0 & 0 & 0 \end{pmatrix} \right] \right\}^{2/5}. \quad (43)$$

The tabulation of  $\phi_f^{(x)}$  is then still useful; the angular terms are unchanged by a change in  $\langle J || Y_2 || J \rangle$  with coupling. Calculation of  $\sigma_1^{(2)}$  using (42) and (43) and computation of the reduced matrix elements in either *LS* or *jj* coupling agrees with the Omont calculation of Sec. VA1. But it is not equal to  $\sigma_1^{(2)}$  using (41) which actually gives  $\sigma_A$  for a  $^1P_1$  state ( $j=l=1$ ).

### 3. Calculation of $\sigma_A(^3P_2)$ and $\sigma_A(^3P_2)/\sigma_A(^3P_1)$

Equations (42) and (43) can be immediately applied to the  $^3P_2$  state yielding  $\sigma_A(^3P_2)/\sigma_A(^3P_1) = 1.35$  in either *LS* or *jj* coupling. This compares with 1.3 given by Omont in his approximation 1.<sup>31</sup> It compares with  $\sigma_A(^1D_2)/\sigma_A(^1P_1) = 1.18$  which one obtains calculating  $\sigma_2^{(2)}/\sigma_1^{(2)}$  using Eq. (41). Omont finds in his second approximation a ratio of 1.14. The above ratios assumed  $\Delta E$  is the same for the  $^3P_1$  and  $^3P_2$  states. Taking  $\Delta E$  equal to the rare-gas energy difference plus 3.04 eV for the 4058-Å transition gives  $\sigma_A(^3P_2)/\sigma_A(^3P_1) \approx (1.36 \text{ to } 1.15)$ . Table IV compares the observed values [row (h)] with the predicted ones [rows (e)–(g)].

The ratio  $\sigma_A(^3P_2)/\sigma_A(^3P_1)$  should be relatively insensitive to the details of the atomic structure. Experimental values are given in Table II. The values obtained by alternation between the two signals at a fixed pressure are more reliable than those deduced from independent measurements of  $\sigma_A(^3P_2)$  and  $\sigma_A(^3P_1)$ . The values lie between the Omont values of 1.36 and 1.15, although the ratio of cross sections found by a nonperturbative solution of Schrödinger's equation and with a numerical integration over impact parameters may not lie between those values. The reduction of the ratio with increasing cross-section size is in contradiction with the earlier argument that the second approximation (predicting 1.15) should be best for small cross sections. But all of the cross sections are small in the sense that they are not much larger than gas kinetic cross sections. The hard-core contributions may then be causing deviations in the expected ratio.<sup>32</sup> Furthermore, the more credible alternation ratios are not inconsistent with the expected 1.15 value for small-impact-parameter collisions. Berman and Lamb found for  $J=1$  that Omont's second-approximation value was much closer to the numerical-integration value than was the result of his first approximation. If the same is true for  $J=2$  the numerical-calculation ratio would be close to 1.15 in agreement with

experiment.

### 4. Calculation of $\sigma_A(^3P_1)$

The disalignment cross sections for the Pb  $^3P_1^o$  excited state can be calculated in *jj* coupling with  $j_a = j_b = \frac{1}{2}$  by applying Eqs. (28), (29), and (36). The  $D$  term vanishes yielding  $\alpha = -\frac{4}{5}e^2(r_{6p,7s})_{av}^2$ . The Slater function approximation of  $r$  is

$$r_{av} = \frac{a_0(n_a^* + n_b^* + 1)}{(Z_a^*/n_a^*) + (Z_b^*/n_b^*)}.$$

For  $6s^26p7s$  one can take  $n_a^* = 4.2$ ,  $n_b^* = 4.3$ ,  $Z_a^* = 6$ , and  $Z_b^* = 1.45$  for which  $(r_{6p,7s})_{av} = 5.38a_0$ . The values of  $P_2^2$  are the same as for the metastables. But  $\Delta E$  may be better approximated by the ionization potential of the rare gas alone since the  $^3P_1^o$  state is connected by strong electric dipole transitions to states both above and below it. The observed values [row (m)] are compared with the Slater-function calculated values [row (i)] in Table IV. The agreement is even poorer than for the metastable states.

The Slater functions contain no nodes so that any interference effects which might reduce  $(r_{6p,7s})_{av}$  are neglected. The lifetime of the  $^3P_1^o$  state against spontaneous decay to the  $6p^2$  configuration is known to be 5.7 nsec.<sup>6</sup> One can then estimate  $(r_{6p,7s})_{av}$  from the relation between lifetime and electric dipole moment<sup>33</sup>:

$$\frac{1}{T_R} = \frac{4}{3} \frac{e^2 \omega^3}{\hbar c^3} |(\tilde{r})|^2.$$

Assuming  $\lambda \approx 3800$  Å since the 3640- and 4058-Å transitions dominate one has  $(r_{6p,7s})_{av} \approx 2.18a_0$ . The resulting cross sections labeled  $T_R$  in Table IV are in much better agreement with experiment.

### B. Wall Relaxation and Non-Maxwellian Velocity Distribution

In Sec. III E it was reported that the measured disalignment times in an evacuated cell,  $T_w(^3P_2) = 41$  μsec and  $T_w(^3P_1) = 49$  μsec, are short compared with the 77-μsec value calculated assuming a uniform spatial distribution initially and complete depolarization with every wall collision. This discrepancy would be removed if the average velocity  $v_{av}$  of the metastable atoms were almost twice that calculated from the known temperature. This is possible since self-reversal and  $^{206}\text{Pb}$  and  $^{207}\text{Pb}$  in the lamp both make the probability of excitation greater for fast ground-state atoms. The introduction of errors into excited-state cross-section measurements by a non-Maxwellian optical excitation has been pointed out previously.<sup>34</sup> It is the relative velocity which appears in the  $(v^{3/5})_{av}/v_{av}$  factor in the average cross section; fortunately  $^{208}\text{Pb}$  is heavy and the relative velocity comes



mostly from the faster lighter perturbing atom in its ground state. But if the average Pb velocity were actually  $\frac{77}{41} = 1.88$  times the Maxwellian value, the average relative velocity would be 16% higher for Kr and 32% higher for Xe. It is likely that the discrepancy between 41 and 77  $\mu\text{sec}$  results at least in part from an initial nonuniform spatial distribution from focusing the lamp output into the cell and absorption in the cell. Nonetheless, the Xe cross sections are suspect; correction for a higher velocity would reduce them making their ratio to the Ar values in better agreement with theory. The metastable quenching cross sections are unaffected by an initial non-Maxwellian velocity since thermalization within the metastable occurs before quenching.

The fact that the evacuated-cell relaxation times for the two metastables are unequal and in the ratio  $T_w(^3P_1)/T_w(^3P_2) = 1.195 \pm 0.029$  is also confusing. Since both states are produced by optical decay from the same excited state, there should be no difference in their velocity distributions. It is possible that the detecting light selects higher-velocity metastables; this could also make  $T_w$  smaller than the 77  $\mu\text{sec}$ . But it would be surprising if the 3683- and 4058- $\text{\AA}$  lines probed very different velocities. Another explanation for the difference in disalignment times comes from noting that the lifetime of the metastable state is 10 or 20 times longer than the disalignment time. Apparently the disalignment occurs not by the atom sticking to the wall but rather by a short-range impact. The wall collision may then be describable by the van der Waals treatment of Omont in Sec. VA. In fact the ratio is reasonably close to the ratio  $\sigma_A(^3P_2)/\sigma_A(^3P_1) = 1.15$  predicted for small-impact-parameter collisions.

### C. Quenching Cross Sections

In Table III it was reported that  $\text{H}_2$  is a better quencher of the  $^3P_1$  metastable state than  $\text{D}_2$  or  $\text{N}_2$  by a factor of 100 or more. But from Table I,  $\text{N}_2$  is at least ten times more effective in quenching the  $^3P_1^o$  excited state than  $\text{H}_2$  or  $\text{D}_2$ . It is interesting to note that the  $^3P_1$  to  $^3P_0$  energy separation of 7819  $\text{cm}^{-1}$  is much closer to the 8083- $\text{cm}^{-1}$  separation between the  $v=0$  and  $v=2$  vibrational states of  $\text{H}_2$  than to the nearest transitions in  $\text{D}_2$  (8605  $\text{cm}^{-1}$  for  $v=0$  to  $v=3$ ) and  $\text{N}_2$  (6905  $\text{cm}^{-1}$  for  $v=0$  to  $v=3$ ). Of course, a meaningful theoretical prediction would involve transitions between the actual molecular potential surfaces of the initial and all possible final states of the composite system. For the rare gases, the transfer or quenching cross sections vanish under the assumptions of Sec. VA; experimentally the cross sections for quenching by the rare gases are much smaller than the correspond-

ing disalignment cross sections.

## VI. CONCLUDING REMARKS

By simple optical techniques the ground state, three metastable states, and one short-lived excited state have been polarized permitting the study of  $g$  values and collisional depolarization and quenching. The cross sections were shown to be in fair agreement with values calculated from the second-order term of the dipolar electrostatic interaction. A direct integration of the Schrödinger equation for which neglect of noncommutativity does not arise has been performed by Berman and Lamb<sup>22</sup> for  $J=1$ . Such a calculation for  $J=2$  would permit a better comparison with theory. The Berman-Lamb formalism avoids the average-energy  $\Delta E$  approximation, but the atomic structures of the colliding atoms need to be known in detail in order to evaluate their expressions for absolute cross sections. An anomalously small cross section has been reported by Schearer for a Ne configuration with an outer  $s$  electron similar to the  $6s^26p7s\ ^3P_1^o$  state of Pb. The smallness of the Ne cross section might be explained by cancellations in evaluating the second-order term involving all possible intermediate states. Schearer<sup>35</sup> reports depolarization cross sections for the  $^3P_2$  states of Ne, Ar, and Xe; all lie within the usual range of 5 to 200  $\text{\AA}^2$  except the  $\text{Ne}(^3P_2)\text{-He}$  cross section which is only 0.43  $\text{\AA}^2$ . The usual treatment of the interaction potential seems incapable of describing this small value, since according to Eq. (29) the atomic structure factor is the product of a contribution from each of the colliding atoms. Crudely, one might argue that neither factor can be small since both the non-resonant  $\text{Ne}(^3P_2)\text{-Ne}(^1S_0)$  cross section (16.6  $\text{\AA}^2$ ) and the  $\text{Ar}(^3P_2)\text{-He}$  and  $\text{Xe}(^3P_2)\text{-He}$  cross sections are large.<sup>35</sup> So how can either  $\alpha(\text{Ne}(^3P_2))$  or  $P_2^2(\text{He})$  be small? One might conclude that the theory of nonresonant collisions with cross sections less than 100  $\text{\AA}^2$  is still much less reliable than that for the much larger ( $10^3$  to  $10^4$   $\text{\AA}^2$ ) cross sections of the theoretically simpler resonant collisions.<sup>23</sup> But the difficulty is likely computational rather than conceptual.

## ACKNOWLEDGMENTS

Thanks are in order to Professor Berken Chang for assisting with the construction of the apparatus and accumulation of excited-state disalignment data and to Dr. C. W. White for contributing to the metastable pumping data. Helpful discussions were held with Dr. P. Berman, Dr. R. Freund, Professor A. Lurio, Professor A. Omont, and Dr. C. W. White. Dedicated technical assistance by George Churchill is particularly appreciated.

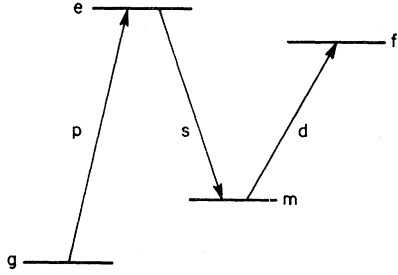


FIG. 19. Energy-level scheme for metastable alignment transient experiments. The letters are abbreviations for ground (g), excited (e), metastable (m), and final (f) states and for pumping (p), scattered (s), and detected (d) radiation.

#### APPENDIX: MULTIPOLE EXPANSION OF METASTABLE ALIGNMENT TRANSIENT SIGNAL

The following derivation is an extension of the calculation by Happer and Saloman<sup>6</sup> for the intensity of fluorescent light in a Hanle experiment. The present problem and nomenclature are pictured in Fig. 19. The intensity of light of polarization  $\hat{d}$  absorbed by atoms in transitions from metastable state  $m$  to final state  $f$  is

$$\bar{I}(\Omega) d\Omega \propto d\Omega \sum_{M_f} \langle M_f | \hat{d} \cdot \vec{D} | \psi_m \rangle \langle \psi_m | \hat{d}^* \cdot \vec{D} | M_f \rangle, \quad (A1)$$

where  $\vec{D}$  is the electric dipole moment operator, and

$$\bar{I}(\Omega) = \langle M_f | \hat{d} \cdot \vec{D} | M'_m \rangle \rho_m(M'_m, M''_m) \langle M''_m | \hat{d}^* \cdot \vec{D} | M_f \rangle, \quad (A2)$$

$$\begin{aligned} \rho_m(M'_m, M''_m) &= \sum_{M_e M'_e M_g s} \int_{\Omega_s} \langle M'_m | \hat{s} \cdot \vec{D} | M_e \rangle \langle M_e | \hat{p} \cdot \vec{D} | M_g \rangle \\ &\times \langle M_g | \hat{p}^* \cdot \vec{D} | M'_e \rangle \langle M'_e | \hat{s}^* \cdot \vec{D} | M''_m \rangle, \quad (A3) \end{aligned}$$

i. e., the metastable density matrix is determined by excitation by radiation of polarization  $\hat{p}$  from an unpolarized ground state  $g$  to excited  $e$  followed by spontaneous emission from the excited state to the metastable state. Since electromagnetic waves are transverse, the polarization vectors  $\hat{s}$  lie in a plane perpendicular to the propagation vector  $\hat{k}$ . For fixed  $\hat{k}$ , and taking  $\hat{s}$  real, we see

$$\sum_s (\hat{s} \cdot \vec{D})(\hat{s} \cdot \vec{D}) = D^2 - (\hat{k} \cdot \vec{D})^2. \quad (A4)$$

Then the angular average over the fluorescence in (A3) is

$$\int_{\Omega_s} \sum_s \hat{s} \cdot \vec{D} \hat{s}^* \cdot \vec{D} = \int_{\Omega_s} D^2 (1 - \cos^2 \theta) = \frac{8}{3} \pi D^2, \quad (A5)$$

where  $\theta$  is the angle between  $\hat{k}$  and  $\vec{D}$ . Then

$$\begin{aligned} \rho_m(M'_m, M''_m) &= \frac{8}{3} \pi \sum_{M_e M'_e} (-1)^q \langle M'_m | D(1, -q) | M_e \rangle \\ &\times \langle M_e | \sum_{M_g} \hat{p} \cdot \vec{D} | M_g \rangle \langle M_g | \hat{p}^* \cdot \vec{D} | M'_e \rangle \\ &\times \langle M'_e | D(1, q) | M''_m \rangle. \quad (A6) \end{aligned}$$

Using Eq. (A8) of Happer and Saloman<sup>6</sup> for the expression in parentheses and the Wigner-Eckart theorem<sup>24</sup> for the matrix elements of  $D$  one has

$$\begin{aligned} \rho_m(M'_m, M''_m) &= \sum_{q', L} \left[ \sum_{M_e M'_e} \begin{pmatrix} J_m & 1 & J_e \\ -M'_m & -q & M_e \end{pmatrix} \begin{pmatrix} J_e & L & J_e \\ -M_e & q' & M'_e \end{pmatrix} \begin{pmatrix} J_e & 1 & J_m \\ -M'_e & q & M'_m \end{pmatrix} (-1)^{q-M_e-M'_e+J_e} \right] \\ &\times (-1)^{q'} P^L(-q') (-1)^{J_m-M'_m} \alpha(J_g, J_e, J_m, L), \quad (A7) \end{aligned}$$

where  $\alpha$  is a factor depending upon the details of the reduced matrix elements but is independent of  $q'$ ,  $M'_m$ , and  $M''_m$ . With Edmonds's equation (6.2.8), the square-bracketed expression in (A7) reduces to the product of a  $3j$  and  $6j$  symbol:

$$\begin{aligned} \rho_m(M'_m, M''_m) &= \sum_{L, q'} (-1)^{q'+L+J_m-M'_m} \begin{pmatrix} J_m & L & J_m \\ -M'_m & q' & M'_m \end{pmatrix} P^L(-q') \begin{pmatrix} J_m & L & J_m \\ J_e & 1 & J_e \end{pmatrix} \alpha \\ &= \sum_L \langle J_m M'_m | P^L \cdot T^L | J_m M''_m \rangle \beta(J_g, J_e, J_m, L), \quad (A8) \end{aligned}$$

where  $\beta$  is independent of the projection  $M'_m$  or  $M''_m$  of  $J_m$  and  $M$  of  $L$ . Equation (A8) is the same form as Eq. (5) of Happer and Saloman; their Eqs. (12)–(16) then apply directly yielding

$$\rho_m(t) \propto \sum_{LM} (-1)^M P_M^L T_M^L \exp[-(\Gamma^{(L)} + iM\omega)t], \quad (A9)$$

i. e., the density matrix may be expanded in multipoles of rank  $L$  and components  $M$ . All of the components of a given rank relax with the same characteristic relaxation rate  $\Gamma^{(L)}$ .

Substituting (A9) into (A2), and using (A8) of Happer and Saloman again

$$\begin{aligned} \bar{I}(\Omega) &\propto \text{Tr} \sum_{M'} (-)^M P_M^L T_M^L \\ &\times \sum_{M'} D_M^{L'} T_{-M}^{L'} \exp[-(\Gamma^{(L)} + iM\omega)t] \\ &= \sum_{LM} (-)^M P_M^L D_M^L \exp[-(\Gamma^{(L)} + iM\omega)t], \quad (\text{A10}) \end{aligned}$$

where, for example,<sup>6</sup>

$$D_M^L = \sum_{\mu} d_{\mu-M}^L (-)^{\mu-M-1} C(11L; \mu, M-\mu). \quad (\text{A11})$$

As shown by Happer and Saloman<sup>6</sup> for the Hanle effect, the metastable transient signals "depend in the same way on the polarization vectors of the light, regardless of the angular momenta of the atomic states involved." In the present experiment the Larmor precession frequency  $\omega$  is about  $10^7$  Hz causing the  $M \neq 0$  terms to average to zero within

the time response of the detector, i.e.,

$$\bar{I}(\Omega) \propto \sum_L P_0^L D_0^L e^{-\Gamma^{(L)} t}. \quad (\text{A12})$$

For unpolarized pumping and detecting light incident along the field we find  $p_0 = d_0 = 0$ ,  $p_{\pm} = d_{\pm} = e^{i\alpha}/\sqrt{2}$  with  $\alpha$  random. Then by (A11),  $P_0^1 = D_0^1 = 0$  and  $P_0^2 = D_0^2 = 1/\sqrt{6}$ . The time dependence of the  $L=0$  moment or total population of the state is negligible in comparison with the much more rapid disalignment. Therefore, the observed time dependence observed in Secs. IIID and IIIE arose from disalignment alone.

For circularly polarized pumping and detecting radiation along the field we find  $p_0 = p_{-1} = d_0 = d_{-1} = 0$ ,  $p_{+1} = d_{+1} = 1$ , i.e.,  $P_0^1 = D_0^1 = 1/\sqrt{2}$  and  $P_0^2 = D_0^2 = 1/\sqrt{6}$ . The signal is then an admixture of orientation and alignment; to determine which predominates one would have to carry through the  $\beta$  term of (A8).

<sup>1</sup>Papers I and II on polarization of Pb vapor have been published and should be corrected as follows: On p. 174 of Paper I [H. M. Gibbs, B. Chang, and R. C. Greenhow, Phys. Rev. **188**, 172 (1969)] multiply  $(\nu - \nu_0)^2$  by 4 in the first part of Eq. (10). The second author of Paper II [H. M. Gibbs and C. W. White, Phys. Rev. **188**, 180 (1969)] is Clark Woody White not C. M. White. In J. Margerie, Compt. Rend. **271**, 209 (1970), it is emphasized that in Papers I and II  $g(\tilde{P}_0)$  was reported and not  $g_I$ . Margerie estimates that these may differ by 1 or 2% as a result of a small hyperfine mixing of the  $^3P_1$  state into the  $^3P_0$  state. But since the  $^3P_1$  state possesses an electronic  $g$  value, the small admixture of  $g_I$  into  $g_I$  is appreciable. Margerie suggests that a measurement of  $g(^1S_0)$  would determine  $g_I$  and the hyperfine coupling coefficient  $a'''$ . The tiny branching ratio to the  $^1S_0$  state from the excited  $^3P_1^o$  state and the weak output of a Pb lamp at the wavelengths absorbed by the  $^1S_0$  state make direct optical pumping formidable. Alternatively, one might determine  $a'''$  by extending the present Zeeman measurements to the hyperfine structure of the  $^3P_1$  and  $^3P_2$  metastables (Lurio and Landman have already measured the  $^1D_2$  hyperfine structure in an atomic beam). The value of  $g_I$  could then be calculated, but the accuracy would be limited by that of the intermediate coupling coefficients  $d_1$  and  $d_2$  of Margerie.

<sup>2</sup>B. Chang and H. Gibbs, Bull. Am. Phys. Soc. **13**, 447 (1968).

<sup>3</sup>H. M. Gibbs and B. Chang, Bull. Am. Phys. Soc. **13**, 1674 (1968); H. M. Gibbs, *Sixth International Conference on the Physics of Electronic and Atomic Collisions* (MIT Press, Cambridge, Mass., 1969), p. 718.

<sup>4</sup>H. M. Gibbs, B. Chang, and R. C. Greenhow, Phys. Rev. Letters **22**, 270 (1969).

<sup>5</sup>The detection of the excited-state alignment via the polarization of the fluorescence follows J. P. Barrat, D. Casalta, J. L. Cojan, and J. Hamel [J. Phys. (Paris) **27**, 608 (1966)].

<sup>6</sup>W. Happer and E. B. Saloman, Phys. Rev. **160**, 23 (1967).

<sup>7</sup>E. B. Saloman and W. Happer, Phys. Rev. **144**, 7 (1966).

<sup>8</sup>Determined from the vapor-pressure table of Ref. 6 and a careful temperature measurement  $T_S$  of the coolest

portion of the Pb sidearm. The sidearm density was multiplied by  $(T_S/T_C)^{1/2}$  to obtain the density in the cell at temperature  $T_C$ .

<sup>9</sup>P. T. Cunningham and J. K. Link, J. Opt. Soc. Am. **57**, 1000 (1967).

<sup>10</sup>At the high densities ( $>10^{14}$  cm<sup>-3</sup>) needed for resonant-collision studies the Pb rapidly effused from the cell. Insertion of the plug stopped the outward flow and increased the cell density by 16% as measured by the fluorescence intensity at low densities. This furnishes an interesting check on the conductance calculations of S. Dushman and J. M. Lafferty, *Scientific Foundations of Vacuum Technique* (Wiley, New York, 1962), pp. 93 and 94. Let the sidearm, cell, and pump tube be denoted by subscripts S, C, and P, respectively. Let  $F_{CP}$  be the conductance from the cell to the pumping tube, etc. Then the cell-density time dependence is

$$\dot{n}_C = -n_C F_{CP} - n_C F_{CS} + n_S F_{SC} + n_P F_{PC}.$$

But  $T_P$  is kept cool so that  $n_P \approx 0$ . Then in equilibrium

$$n_C = \frac{F_{SC}}{F_{CP} + F_{CS}} \quad n_S = \frac{n_C}{(1 + F_{CP}/F_{CS})},$$

since  $F_{SC} = F_{CS}$ . With both capillaries at  $T_C$ ,  $F_{CP}/F_{CS} = K_{CP}/K_{CS}$ , where  $K$  is Clausing's factor and depends upon geometry. For  $K_{CP}$ ,  $l/a = 4.75$  cm/0.05 cm  $\approx 95$  so  $K = 0.0271$  from Dushman's Table 2.2. For  $K_{CS}$ ,  $l/a \approx 0.635/0.05 = 12.7$ , so  $K_{CS} \approx 0.165$ . Then without the plug  $n_C = n_S/1.164$ ; with the plug  $F_{CP} \approx 0$  and  $n'_C \approx n_S$ , i.e.,  $n'_C/n_C = 1.16$ .

<sup>11</sup>The trapping probability  $x$  is difficult to calculate because it depends upon the geometrical details of the cell and excitation beam. The approximate expression given in M. I. D'yakonov and V. I. Perel, Zh. Eksperim. i Teor. Fiz. **47**, 1483 (1964) [Sov. Phys. JETP **20**, 997 (1965)], is

$$x \approx 1 - \frac{1}{\sqrt{\pi}} \int_{-\infty}^{\infty} e^{-t^2} \left[ e^{-(L/t_0)e^{-t^2}} \right] dt,$$

where  $L$  is a characteristic dimension of the cell and  $l_0$  is the trapping length  $(2j_0 + 1)8\pi^{3/2}v_0/(2j_1 + 1)n_0\lambda^3\gamma$ , where  $j_0$  and  $j_1$  are the ground- and excited-state total angular

momenta, respectively;  $v_0$  is the most probable speed;  $n_0$  is the ground-state density;  $\lambda$  is the light wavelength; and  $\gamma$  is the reciprocal lifetime. For  $n_0 \approx 10^{11} \text{ cm}^{-3}$ ,  $l_0 \approx 10$ ,  $L < l_0$  so  $x \approx L/\sqrt{2}l_0 \leq 0.07$  for  $L \leq 1 \text{ cm}$ , and  $xR \approx 0.019$ . Usually  $n_0 \approx 3.5 \times 10^{10} \text{ cm}^{-3}$  so that  $xR$  was less than 0.01 for the foreign-gas data. Experimentally there appeared to be little change in  $S$  below  $5 \times 10^{11} \text{ cm}^{-3}$ . For  $L \gg l_0$ ,  $x \approx 1 - l_0 L^{-1} [\pi \ln(L/l_0)]^{-1/2}$ . The  $R$  and  $\sigma v$  flow-lamp data were taken for  $n_0 > 10^{14} \text{ cm}^{-3}$  implying  $l_0 < 10^{-2}$  and  $x > 0.98$  even for an  $L$  of only 2 mm as a result of masking (see Ref. 13). For the  $R$  determination with a buffer gas  $n_0 \approx 10^{13}$  and  $L \approx 1 \text{ cm}$  since little masking was used so  $x \approx 0.96$ .

<sup>12</sup>D. R. Jenkins, Proc. Roy. Soc. (London) **A313**, 551 (1969).

<sup>13</sup>N. P. Penkin and I. Slavenas, Opt. i Spektroskopiya **15**, 154 (1963) [Opt. Spectry. **15**, 83 (1963)], report  $R=0.3$ . Our data taken with a flow lamp to increase the intensity and permit a smaller detection solid angle yield  $R \approx 0.32$  and  $\sigma v \approx 6.4 \times 10^{-8} \text{ cm}^3/\text{sec}$  but the uncertainty in  $R$  is about 25% and about 50% for  $\sigma v$  because no extrapolation to zero solid angle was made.

<sup>14</sup>A. Lurio and D. A. Landman, in *Proceedings of the International Colloquium No. 164 on the Magnetic Hyperfine Structure of Atoms and Molecules, Paris*, 1966 (Centre National de la Recherche Scientifique, Paris, 1967), p. 217; G. V. Oppen, Z. Physik **213**, 261 (1968).

<sup>15</sup>A. Lurio and D. A. Landman, J. Opt. Soc. Am. **60**, 759 (1970).

<sup>16</sup>The uncertainty  $\sigma$  is three times the standard deviation  $\sigma_M$  of the mean, i. e.,

$$\sigma = 3\sigma_M = 3\left\{\sum_i (v_i - \bar{v})^2 / [n(n-1)]\right\}^{1/2},$$

where  $n$  is the number of measurements.

<sup>17</sup>B. Cagnac, Ann. Phys. (Paris) **6**, 467 (1961).

<sup>18</sup>Theoretically  $T_R$  for the  $^1D_2$ ,  $^3P_2$ , and  $^3P_1$  states are 0.037, 2.6, and 0.137 sec, respectively: R. H. Garstang, J. Res. Natl. Bur. Std. **68A**, 61 (1964).

<sup>19</sup>A. Gallagher and A. Lurio, Bull. Am. Phys. Soc. **7**, 258 (1962); J. A. Bellisio and P. Davidovits, *ibid.* **15**, 558 (1970); H. M. Gibbs, G. G. Churchill, T. R. Marshall, J. F. Papp, and F. A. Franz, Phys. Rev. Letters **25**, 263 (1970).

<sup>20</sup>In Baumann's article [M. Baumann, Z. Physik **173**, 519 (1963)] the  $\text{Hg}(6^3P_2)$  metastable lifetime was found to be one or two orders of magnitude longer than the disorientation time over the range  $2 \times 10^{-3}$  to  $2 \times 10^{-2}$  Torr.

<sup>21</sup>W. E. Deming, *Statistical Adjustment of Data* (Wiley, New York, 1943), pp. 166–168.

<sup>22</sup>P. R. Berman and W. E. Lamb, Jr., Phys. Rev. **187**, 221 (1969). In the notation of Eq. (28) divide Berman and Lamb's row  $\Gamma_2^N$  of Table VI by 2.7 (their methods 1 and 3 correspond to Omont's 2 and 1, respectively), yielding  $C=1.82$  to 2.67 in Omont's approximation [P. R. Berman (private communication)].

<sup>23</sup>A. Omont, J. Phys. (Paris) **26**, 26 (1965). For a resonant broadening numerical calculation with fewer approximations see, A. Omont and J. Meunier, Phys. Rev. **169**, 92 (1968).

<sup>24</sup>A. R. Edmonds, *Angular Momentum in Quantum Mechanics* (Princeton U. P., Princeton, N. J., 1957).

<sup>25</sup>D. R. Wood and K. L. Andrew, J. Opt. Soc. Am. **58**, 818 (1968).

<sup>26</sup>J. C. Slater, Phys. Rev. **36**, 57 (1930).

<sup>27</sup>T. Hänsch, R. Odenwald, and P. Toschek, Z. Physik **209**, 478 (1968), Eqs. (40) and (41).

<sup>28</sup>F. Herman and S. Skillman, *Atomic Structure Calculations* (Prentice-Hall, Englewood Cliffs, N. J., 1963).

<sup>29</sup>J.-P. Faroux, These de Doctorat (Laboratoire de Physique, Ecole Normale Supérieure, 1969), p. 75 (unpublished); A. Dalgarno and A. E. Kingston, Proc. Roy. Soc. (London) **A259**, 424 (1960).

<sup>30</sup>C. H. Wang and W. J. Tomlinson, Phys. Rev. **181**, 115 (1969). There seem to be several confusing errors including: the  $-1$  superscript  $l$  in (31) and (32) should be  $j$ ; the summations in (41) are from  $x=0$  to  $x=2j$ ; Eq. (45) is  $\lambda_a = \delta_a B_l / b_l^3$ .

<sup>31</sup>Calculated in  $LS$  coupling, A. Omont (private communications).

<sup>32</sup>J.-P. Faroux and J. Brossel, Compt. Rend. **265**, 1412 (1967); and Ref. 29.

<sup>33</sup>L. I. Schiff, *Quantum Mechanics*, 2nd ed. (McGraw-Hill, New York, 1955), p. 261.

<sup>34</sup>See p. A622 of F. W. Byron, Jr., M. N. McDermott, and R. Novick, Phys. Rev. **134**, A615 (1964).

<sup>35</sup>L. D. Scheerer, Phys. Rev. **188**, 505 (1969).